

Structure of the ground and excited states in ${}^9_{\Lambda}\text{Be}$ nucleus

A. V. Nesterov, Yu. A. Lashko*, V. S. Vasilevsky

*Bogolyubov Institute for Theoretical Physics,
Kiev 03143, Ukraine*

Abstract

We investigate properties of bound and resonance states in the ${}^9_{\Lambda}\text{Be}$ nucleus. To reveal the nature of these states, we use a three-cluster $2\alpha + \Lambda$ microscopic model. The model incorporates Gaussian and oscillator basis functions and reduces a three-cluster Schrödinger equation to a two-body like many-channel problem with the two-cluster subsystems (${}^5_{\Lambda}\text{He}$ and ${}^8\text{Be}$) being in a bound or a pseudo-bound state. Influence of the cluster polarization on the energy and widths of resonance states in ${}^9_{\Lambda}\text{Be}$ and on elastic and inelastic ${}^5_{\Lambda}\text{He} + \alpha$ scattering is analysed.

Keywords:

Cluster model, Resonating Group Method, hypernucleus, three-cluster microscopic model, cluster polarization, resonance states

PACS: 21.60.Gx, 21.60.-n, 24.10.-i

1. Introduction

We apply a microscopic three-cluster model to study the hypernucleus ${}^9_{\Lambda}\text{Be}$. This nucleus is considered as a three-cluster system $\alpha + \alpha + \Lambda$. Our aim is to examine both discrete and continuous spectrum states of ${}^9_{\Lambda}\text{Be}$. This research is performed within a microscopic three-cluster model referred as AMGOB (the Algebraic Model of scattering with the Gaussian and Oscillator Bases). This model was formulated in Ref. [1]. In Refs. [1, 2, 3, 4, 5],

*
Email addresses: nesterov@bitp.kiev.ua (A. V. Nesterov), ylashko@gmail.com (Yu. A. Lashko), vsvasilevsky@gmail.com (V. S. Vasilevsky)

the AMGOB has been successfully applied to study structure of bound and resonance states in the light nuclei ${}^7\text{Be}$, ${}^7\text{Li}$, ${}^8\text{Li}$, ${}^8\text{B}$, ${}^{10}\text{Be}$ and ${}^{10}\text{B}$. The model has been also applied in Ref. [6] to study the astrophysical S factors of the capture reactions of astrophysical importance. By this reason, the model is particularly appealing for investigating different two-body decay channels of the compound hypernucleus.

The energy of $1/2^+$ ground state in ${}^9_{\Lambda}\text{Be}$ is -3.12 MeV with respect to its lowest binary decay threshold ${}^9_{\Lambda}\text{Be} \rightarrow {}^5_{\Lambda}\text{He} + \alpha$ and -6.63 MeV relative to its three-cluster $2\alpha + \Lambda$ threshold. Unlike ${}^9\text{Be}$, which is a Borromean nucleus, ${}^9_{\Lambda}\text{Be}$ has a bound two-body subsystem ${}^5_{\Lambda}\text{He}$. That is why it is important to take into account the possibility for the ${}^9_{\Lambda}\text{Be}$ hypernucleus to decay via ${}^9_{\Lambda}\text{Be} \rightarrow {}^5_{\Lambda}\text{He} + \alpha$ channel. The ground state of ${}^8\text{Be}$ subsystem is known to be a very narrow resonance just near 2α threshold. Hence space correlations between α -particles should also be considered properly. AMGOB model gives us a possibility to take into account two coupled binary cluster configurations ${}^5_{\Lambda}\text{He} + \alpha$ and ${}^8\text{Be} + \Lambda$ allowing for ${}^5_{\Lambda}\text{He}$ and ${}^8\text{Be}$ to be polarized. The term "cluster polarization" connotes changing energy of a two-cluster subsystem (and, hence, change of its shape and/or size) due to the interaction with the third cluster.

The light hypernuclei have been investigated within different models in Refs. [7, 8, 9, 10, 11, 12, 13, 14, 15, 16, 17, 18, 19, 20, 21, 22, 23, 24, 25, 26, 27, 28, 29]. In Ref. [11] $L^\pi = 0^+$ ground state and $L^\pi = 2^+$ excited states of ${}^9_{\Lambda}\text{Be}$ have been investigated with a microscopic cluster model. Spin of a Λ -hyperon was disregarded in [11] and, hence, all the states of ${}^9_{\Lambda}\text{Be}$ hypernucleus have been classified with the values of the total orbital momentum L . For the description of the core nucleus ${}^8\text{Be}$ the generator coordinate method of a microscopic 2α cluster model has been applied. The Λ -nucleus potentials have been constructed by folding ΛN interactions with the nuclear density calculated by the microscopic cluster model. A core polarization has been taken into account by artificial enhancing the central part of NN -potential. In this assumption, strengthening of the effective central nuclear interactions acts like an intensification of the inter-cluster potentials. This procedure simulates an additional attraction to the nuclear system from ΛN interaction. The optimum value of the enhancement factor was chosen to minimize the energy of the total system. Authors claimed that particularly remarkable core polarization effects are found in ${}^9_{\Lambda}\text{Be}$, because ${}^8\text{Be}$ is a very fragile system of the quasi-bound 2α state. The core polarization effects have been seen in the nuclear size change and the energy changes caused by the Λ -particle in ${}^9_{\Lambda}\text{Be}$.

The significant shrinkage of 2α structure in ${}^9_{\Lambda}\text{Be}$ has also been reported.

In Ref. [30] energy spectra of bound and resonance states of ${}^9_{\Lambda}\text{Be}$ have been calculated within the framework of $\alpha+\alpha+\Lambda$ three-body model. The $\alpha-\alpha$ interaction was chosen so to reproduce the observed $\alpha-\alpha$ scattering phase shift and the ground state of ${}^8\text{Be}$ within the $\alpha-\alpha$ orthogonality condition model. The $\Lambda\alpha$ interaction was obtained by folding the ΛN interaction into the α cluster wave function. Even- and odd-states of ΛN interaction have been adjusted so as to reproduce the observed binding energies of the ground states in ${}^5_{\Lambda}\text{He}$ and ${}^9_{\Lambda}\text{Be}$. For the resonant states of ${}^9_{\Lambda}\text{Be}$ the complex scaling method has been employed. The level structure has been categorized into ${}^8\text{Be}$ -analogue states, genuine hypernuclear states, ${}^9\text{Be}$ analogue states, which have already been discussed in [31, 32, 33] and some new states located at more than 10 MeV above the $\alpha+\alpha+\Lambda$ threshold states.

An extensive discussion of the structure of genuine hypernuclear states of ${}^9_{\Lambda}\text{Be}$, as well as ${}^8\text{Be}^*$ -analogue states, within a microscopic $\alpha+\alpha(\alpha^*)+\Lambda$ cluster model is given also in review paper [7].

In Ref. [34] ${}^9_{\Lambda}\text{Be}$ hypernucleus has been treated as the $S=1/2$, $T=0$ bound state of the three-cluster system $\alpha\alpha\Lambda$. The cluster-reduction method is used to solve the s-wave differential Faddeev equations. Phenomenological potentials have been used to describe $\Lambda\alpha$ and $\alpha\alpha$ interactions. The authors have considered boundary-value problems corresponding to the bound states in the $\alpha\alpha\Lambda$ system and the problems of low-energy alpha-particle scattering on a ${}^5_{\Lambda}\text{He}$ hypernucleus. The s-wave phase shift for $\alpha-{}^5_{\Lambda}\text{He}$ scattering has been shown to behave anomalously at energies of relative motion below 1 MeV being small and positive. The scattering length has been observed to be large in magnitude and negative, which has been attributed by the authors to the presence of a virtual level in the $\alpha\alpha\Lambda$ system near the threshold for scattering.

In [35] the first ab initio calculations for p-shell single- Λ hypernuclei using no-core shell model approaches with explicit hyperons have been presented. In addition to chiral two- and three-nucleon interactions, they used leading-order (LO) chiral hyperon-nucleon (YN) interactions and a meson-exchange hyperon-nucleon interaction. They have shown that the chiral hyperon-nucleon interactions provide the ground-state and excitation energies that generally agree with experiment within the cutoff dependence. At the same time they demonstrated that hypernuclear spectroscopy provides tight constraints on the hyperon-nucleon interactions. A peculiarity of ${}^9_{\Lambda}\text{Be}$ is that the spin-doublet resulting from the 2^+ state in ${}^8\text{Be}$ is practically degenerate, with

the higher J state being at slightly lower excitation energy experimentally, contrary to other light hypernuclei. The LO chiral YN interactions reproduce the excitation energy of the doublet and the near degeneracy within threshold extrapolation and convergence uncertainties. However, the order of levels is wrong. In contrast, the Julich'04 interaction [36] gives a significant splitting of the spin doublet in contradiction to experiment.

The energy splitting of the $5/2_1^+ - 3/2_1^+$ doublet states in ${}^9_\Lambda\text{Be}$, which was considered to be dominantly composed of the ${}^8\text{Be}(2_1^+) \otimes \Lambda(s_{1/2})$ configuration, has been studied in [16] within a microscopic three-body model $2\alpha + \Lambda$. The Pauli principle between two α clusters has been taken into account by the orthogonality condition model. The main purpose of Ref. [16] was to demonstrate how the splitting of the spin-doublet states in ${}^9_\Lambda\text{Be}$ is related to the underlying LS and antisymmetric LS forces (ALS), which are different between one-boson-exchange models and quark models. The quark model predicts that the ALS component of the LN interaction is so strong as to substantially cancel the LS one, while the one-boson-exchange models propose much smaller ALS and various strength of LS. The $\Lambda\alpha$ interactions are derived by folding the ΛN interaction into the density of the α cluster. The authors introduced a phenomenological ΛNN three-body force, folding of which leads to both $\Lambda\alpha\alpha$ and $\Lambda\alpha$ potentials. All the available Nijmegen one-boson-exchange model ΛN interactions lead to a wide range of splittings of 0.08-0.20 MeV in ${}^9_\Lambda\text{Be}$. At the same time, quark-model ΛN interactions, which have generally large ALS force, gives a half of the smallest one-boson-exchange model prediction for the splitting. These data are compatible with the experimental results reported in [17].

Based on the Faddeev methodology calculations of $2\alpha + \Lambda$ system, which used two-cluster resonating-group method kernels, have been performed in Ref. [27]. The method, which was used in [27], is equivalent to the pairwise orthogonality condition model of three-cluster systems, interacting via two-cluster RGM kernels. The three-range Minnesota force, which describes the $\alpha\alpha$ phase shifts, has been chosen as an effective two-nucleon interaction. A simple two-range Gaussian potential for each spin-singlet and spin-triplet state, generated from the phase-shift behavior of the quark-model hyperon-nucleon interaction, has been used as a ΛN force for $\Lambda\alpha$ interaction. To solve the Faddeev equation, the authors discretized the continuous momentum variable for the Jacobi coordinate vectors. The authors stated that the $L^\pi = 0^+$ ground state and the $L^\pi = 2^+$ excited state of ${}^9_\Lambda\text{Be}$ are well described by the contracted 2α cluster structure with a weakly coupled Λ -particle in

the dominant s -wave component. However, the energy gain for ${}^9_\Lambda\text{Be}$ due to partial waves higher than the s -wave is claimed to be about 1.2 MeV, because oscillatory behavior of the $\alpha\alpha$ relative wave functions needs more partial waves with a larger energy gain.

In the present paper the structure of bound and resonance states in ${}^9_\Lambda\text{Be}$ hypernucleus for the states $1/2 \leq J \leq 7/2$ of positive and negative parity is investigated with special emphasis on the impact of cluster polarization on the spectrum of the ${}^9_\Lambda\text{Be}$ and elements of scattering matrix. The Pauli exclusion principle between α -clusters is taken into account completely. We employ an effective ΛN single-channel interaction simulating the basic features of the Nijmegen meson-theoretical models NSC97f [16], in which a cut-off parameter k_F was adopted to reproduce the energy of the ground state of ${}^9_\Lambda\text{Be}$ with respect to $2\alpha + \Lambda$ threshold. As a NN interaction the modified Hasegawa-Nagata potential is chosen with the Majorana parameter being adjusted to give the experimentally observed energy of ${}^9\text{Be}$ nucleus. Parameters of resonance states are determined from analysis of the energy dependence of two-channel S -matrix for $\alpha-{}^5_\Lambda\text{He}$ and $\Lambda-{}^8\text{Be}$ scattering, provided that ${}^5_\Lambda\text{He}$ and ${}^8\text{Be}$ subsystems being in their ground states in entrance and exit channels.

The paper is organized as follows. Formulation of a microscopic three-cluster model used for the investigation of the ${}^9_\Lambda\text{Be}$ hypernucleus is given in Section 2. In Section 3 we analyze how the spectrum of bound and resonance states of ${}^9_\Lambda\text{Be}$ depends on the polarization of two-cluster subsystems ${}^5_\Lambda\text{He}$ and ${}^8\text{Be}$. The nature of the obtained resonance states in ${}^9_\Lambda\text{Be}$ is also discussed in Section 3. Conclusions are made in Section 4.

2. Formulation of the model

Let us consider a microscopic Hamiltonian for a system consisting of 8 nucleons (two alpha-particles) and a Λ hyperon:

$$\begin{aligned} \hat{H} = & -\frac{\hbar^2}{2m} \sum_{i=1}^8 \frac{\partial^2}{\partial \mathbf{r}_i^2} - \frac{\hbar^2}{2m_\Lambda} \frac{\partial^2}{\partial \mathbf{r}_\Lambda^2} \\ & + \sum_{i<j}^8 V_{NN}(\mathbf{r}_i - \mathbf{r}_j) + \sum_{i=1}^8 V_{N\Lambda}(\mathbf{r}_i - \mathbf{r}_\Lambda) \end{aligned} \quad (1)$$

where $m = (938.272 + 939.565)/2 = 938.919 \text{ MeV}/c^2$ is a nucleon mass and $m_\Lambda = 1115.683(6) \text{ MeV}/c^2$ is a mass of the Λ hyperon. It is more expedient

to use the mass of a nucleon m as a unit mass and than the mass of the hyperon $\bar{m}_\Lambda = m_\Lambda/m = 1.18826$. It is assumed that coordinates of nucleons and a coordinate of the hyperon are determined in the center-of-mass system, and thus center of mass motion is eliminated from the Hamiltonian.

The total Hamiltonian can be separated into nuclear and hypernuclear parts:

$$\begin{aligned}\hat{H} &= \hat{H}_{NN} + \hat{H}_{N\Lambda}, \\ \hat{H}_{NN} &= -\frac{\hbar^2}{2m} \sum_{i=1}^8 \frac{\partial^2}{\partial \mathbf{r}_i^2} + \sum_{i<j}^8 V_{NN}(\mathbf{r}_i - \mathbf{r}_j),\end{aligned}\quad (2)$$

$$\hat{H}_{N\Lambda} = -\frac{\hbar^2}{2m_\Lambda} \frac{\partial^2}{\partial \mathbf{r}_\Lambda^2} + \sum_{i=1}^8 V_{N\Lambda}(\mathbf{r}_i - \mathbf{r}_\Lambda). \quad (3)$$

Eigenfunctions of Hamiltonian (1) characterized with the total angular momentum J and energy E of the relative motion of the cluster will be sought in the form:

$$\begin{aligned}\Psi_{EJ} &= \sum_L \sum_{\alpha=1}^2 \sum_{\lambda_\alpha, l_\alpha} \hat{\mathcal{A}} \{ \Phi_1(^4He) \Phi_2(^4He) \Phi_3(\Lambda) \\ &\times f_{\lambda_\alpha, l_\alpha; L}^{(E, J)}(x_\alpha, y_\alpha) \{ Y_{\lambda_\alpha}(\hat{\mathbf{x}}_\alpha) Y_{l_\alpha}(\hat{\mathbf{y}}_\alpha) \}_L \}_{JM_J}.\end{aligned}\quad (4)$$

Here we involve two Faddeev amplitudes $f_{\lambda_\alpha, l_\alpha; L}^{(E, J)}(x_\alpha, y_\alpha)$ which represent dynamics in binary channels ${}^5_\Lambda\text{He} + \alpha$ ($\alpha=1$) and ${}^8\text{Be} + \Lambda$ ($\alpha=2$). The Jacobi vector \mathbf{x}_1 ($=x_1 \cdot \hat{\mathbf{x}}_1$) determines distance between an alpha particle and a Λ -hyperon:

$$\mathbf{x}_1 = \sqrt{\frac{4\bar{m}_\Lambda}{\bar{m}_\Lambda + 4}} \left[\mathbf{r}_\Lambda - \frac{1}{4} \sum_{i=1}^4 \mathbf{r}_i \right], \quad (5)$$

while the Jacobi vector \mathbf{y}_1 is the distance between an alpha particle and ${}^5_\Lambda\text{He}$ binary subsystem:

$$\mathbf{y}_1 = \sqrt{\frac{4(\bar{m}_\Lambda + 4)}{\bar{m}_\Lambda + 8}} \left[\frac{1}{4} \sum_{i=5}^8 \mathbf{r}_i - \frac{1}{\bar{m}_\Lambda + 4} \left(\mathbf{r}_\Lambda + \sum_{i=1}^4 \mathbf{r}_i \right) \right] \quad (6)$$

The second tree of Jacobi coordinates involves vector \mathbf{x}_2 , which describes the

relative distance between two alpha particles,

$$\mathbf{x}_2 = \sqrt{2} \left[\frac{1}{4} \sum_{i=1}^4 \mathbf{r}_i - \frac{1}{4} \sum_{j=5}^8 \mathbf{r}_j \right] \quad (7)$$

and vector \mathbf{y}_2 , which determines position of the Λ -hyperon relative to the ${}^8\text{Be}$:

$$\mathbf{y}_2 = \sqrt{\frac{8\bar{m}_\Lambda}{\bar{m}_\Lambda + 8}} \left[\mathbf{r}_\Lambda - \frac{1}{8} \sum_{i=1}^8 \mathbf{r}_i \right] \quad (8)$$

It is worthwhile underlining that the antisymmetrization operator $\widehat{\mathcal{A}}$ in (4) permutes coordinates of nucleons only. It does not involve a hyperon. Due to this fact, in the second Jacobi tree adopted for describing the channel ${}^8\text{Be}+\Lambda$ we have got a folding type of function Ψ_{EJ} in (4) with the wave function of ${}^8\text{Be}$ being antisymmetric. In the first Jacobi tree associated with the channels ${}^5_\Lambda\text{He}+\alpha$ the antisymmetrization operator $\widehat{\mathcal{A}}$ invokes the exchange of nucleons between ${}^5_\Lambda\text{He}$ and an alpha particle and thus makes antisymmetric a wave function of the compound system ${}^9_\Lambda\text{Be}$.

Equation (4) represents the wave function in the LS coupling scheme. Partial orbital momentum λ_α indicates an internal orbital momentum of ${}^5_\Lambda\text{He}$ ($\alpha=1$) or ${}^8\text{Be}$ ($\alpha=2$), while orbital momentum l_α describes rotation of an alpha particle around ${}^5_\Lambda\text{He}$ ($\alpha=1$) or rotation of the Λ -hyperon around ${}^8\text{Be}$ ($\alpha=2$). The total orbital momentum L is a vector sum of partial orbital momenta: $\vec{L} = \vec{\lambda}_\alpha + \vec{l}_\alpha$. Since the spins of alpha-clusters are equal to zero, the total spin of the hypernucleus ${}^9_\Lambda\text{Be}$ is determined by the spin of the Λ -hyperon and equals $1/2$. Thus with a given value of the total angular momentum J the total orbital momentum L can have two values $L = J - 1/2$ and $L = J + 1/2$. It is true for all values of J and parity π except when $J^\pi = 1/2^-$ where the total orbital momentum has only one value $L = 1$.

Faddeev three-cluster amplitudes $f_{\lambda_\alpha, l_\alpha; L}^{(E, J)}(x_\alpha, y_\alpha)$ are the solutions of an infinite set of integro-differential equations resulting from Schrödinger equation for the wave function (4) with the Hamiltonian (1):

$$\begin{aligned} & \left[\widehat{T}_{x_\alpha, \lambda_\alpha} + \widehat{T}_{y_\alpha, l_\alpha} - E \right] f_{\lambda_\alpha, l_\alpha; L}^{(E, J)}(x_\alpha, y_\alpha) \\ & + \sum_{\beta=1}^2 \sum_{\lambda_\beta, l_\beta} \int_0^\infty \int_0^\infty d\tilde{x}_\beta \tilde{x}_\beta^2 d\tilde{y}_\beta \tilde{y}_\beta^2 \mathcal{V}_{\lambda_\alpha, l_\alpha; \lambda_\beta, l_\beta}^{(L)}(x_\alpha, y_\alpha; \tilde{x}_\beta, \tilde{y}_\beta) \cdot f_{\lambda_\beta, l_\beta; L}^{(E, J)}(\tilde{x}_\beta, \tilde{y}_\beta) \quad (9) \end{aligned}$$

$$= E \sum_{\beta=1}^2 \sum_{\lambda_{\beta}, l_{\beta}} \int_0^{\infty} \int_0^{\infty} d\tilde{x}_{\beta} \tilde{x}_{\beta}^2 d\tilde{y}_{\beta} \tilde{y}_{\beta}^2 \mathcal{N}_{\lambda_{\alpha}, l_{\alpha}; \lambda_{\beta}, l_{\beta}}^{(L)}(x_{\alpha}, y_{\alpha}; \tilde{x}_{\beta}, \tilde{y}_{\beta}) \cdot f_{\lambda_{\beta}, l_{\beta}; L}^{(E, J)}(\tilde{x}_{\beta}, \tilde{y}_{\beta}),$$

where

$$\hat{T}_{z, l} = -\frac{\hbar^2}{2m} \left[\frac{d^2}{dz^2} + \frac{2}{z} \frac{d}{dz} - \frac{l(l+1)}{z^2} \right]$$

is the kinetic energy operator associated with the Jacobi vector $\mathbf{z} = \mathbf{x}_{\alpha}$ or $\mathbf{z} = \mathbf{y}_{\alpha}$, $\mathcal{N}_{\lambda_{\alpha}, l_{\alpha}; \lambda_{\beta}, l_{\beta}}^{(L)}$ is the exchange part of the norm kernel, and $\mathcal{V}_{\lambda_{\alpha}, l_{\alpha}; \lambda_{\beta}, l_{\beta}}^{(L)}$ contains a direct and an exchange part of the potential energy and an exchange term of the kinetic energy of the three-cluster system.

We can reduce a three-cluster problem to a many-channel two-body problem by expanding the wave function $f_{\lambda_{\alpha}, l_{\alpha}; L}^{(E, J)}(x_{\alpha}, y_{\alpha})$ into the basis of eigenfunctions of the two-cluster Hamiltonian consisting of bound states $g_{\mathcal{E}_{\alpha}^{\sigma} \lambda_{\alpha}}(x_{\alpha})$ ($\sigma = 1, 2, \dots$) and continuous spectrum states $g_{\mathcal{E}_{\alpha} \lambda_{\alpha}}(x_{\alpha})$:

$$\begin{aligned} f_{\lambda_{\alpha}, l_{\alpha}; L}^{(E, J)}(x_{\alpha}, y_{\alpha}) &= \sum_{\sigma} g_{\mathcal{E}_{\alpha}^{\sigma} \lambda_{\alpha}}(x_{\alpha}) \cdot \phi_{E - \mathcal{E}_{\alpha}^{\sigma}, l_{\alpha}}(y_{\alpha}) \\ &+ \int d\mathcal{E}_{\alpha} g_{\mathcal{E}_{\alpha} \lambda_{\alpha}}(x_{\alpha}) \phi_{E - \mathcal{E}_{\alpha}, l_{\alpha}}(y_{\alpha}). \end{aligned} \quad (10)$$

Functions $g_{\mathcal{E}_{\alpha}^{\sigma} \lambda_{\alpha}}(x_{\alpha})$ and $g_{\mathcal{E}_{\alpha} \lambda_{\alpha}}(x_{\alpha})$ satisfy the two-cluster Schrödinger equation:

$$\begin{aligned} &\left[\hat{T}_{x_{\alpha}, \lambda_{\alpha}} - \mathcal{E}_{\alpha} \right] g_{\mathcal{E}_{\alpha} \lambda_{\alpha}}(x_{\alpha}) \\ &+ \int_0^{\infty} d\tilde{x}_{\alpha} \tilde{x}_{\alpha}^2 \cdot \mathcal{V}^{(\lambda_{\alpha})}(x_{\alpha}; \tilde{x}_{\alpha}) \cdot g_{\mathcal{E}_{\alpha} \lambda_{\alpha}}(\tilde{x}_{\alpha}) \\ &= \mathcal{E}_{\alpha} \int_0^{\infty} d\tilde{x}_{\alpha} \tilde{x}_{\alpha}^2 \cdot \mathcal{N}^{(\lambda_{\alpha})}(x_{\alpha}; \tilde{x}_{\alpha}) \cdot g_{\mathcal{E}_{\alpha} \lambda_{\alpha}}(\tilde{x}_{\alpha}). \end{aligned} \quad (11)$$

Functions $\phi_{E - \mathcal{E}_{\alpha}^{\sigma}, l_{\alpha}}(y_{\alpha})$ and $\phi_{E - \mathcal{E}_{\alpha}, l_{\alpha}}(y_{\alpha})$ describe scattering of the third cluster on a two-cluster bound state with energy $\mathcal{E}_{\alpha}^{\sigma}$ or a continuum spectrum state with energy \mathcal{E}_{α} , correspondingly. Quantities $\mathcal{N}^{(\lambda_{\alpha})}(x_{\alpha}; \tilde{x}_{\alpha})$ and $\mathcal{V}^{(\lambda_{\alpha})}(x_{\alpha}; \tilde{x}_{\alpha})$ have the same meaning as the similar quantities in Eq. (9), but for two-cluster systems.

So, first we solve two-cluster equation (11) and then use the eigenfunctions of the two-cluster Hamiltonian to find wave functions $\phi_{E - \mathcal{E}_{\alpha}^{\sigma}, l_{\alpha}}(y_{\alpha})$ and $\phi_{E - \mathcal{E}_{\alpha}, l_{\alpha}}(y_{\alpha})$. Finally, we get three-cluster wave function $f_{\lambda_{\alpha}, l_{\alpha}; L}^{(E, J)}(x_{\alpha}, y_{\alpha})$.

In practical calculations the integral part of the expansion (10) is substituted with the sum over the finite number of the discretized states in two-cluster continuum. The more terms in this sum are, the better cluster polarization is taken into account.

As in [4], we use a finite number of square-integrable Gaussian functions to expand two-cluster wave function $g_{\mathcal{E}\lambda_\alpha}(x_\alpha)$:

$$g_{\mathcal{E}\lambda_\alpha}(x_\alpha) = \sum_{\nu=1}^{N_G^{max}} D_\nu^{(\mathcal{E}\lambda_\alpha)} G_{\lambda_\alpha}(x_\alpha, b_\nu), \quad (12)$$

where

$$G_\lambda(\mathbf{x}, b_\nu) = \sqrt{\frac{2}{b_\nu^3 \Gamma(\lambda_\alpha + 3/2)}} \rho^{\lambda_\alpha} \exp\left\{-\frac{1}{2}\rho^2\right\}, \quad (13)$$

$$\left(\rho = \frac{x}{b_\nu}\right)$$

is a Gaussian function. Parameters b_ν are chosen so to minimize the ground state energies of the two-body subsystems.

To find wave functions $\phi_{E-\mathcal{E}, l_\alpha}(y_\alpha)$ of the third cluster interacting with the two-cluster subsystem numerated by index α ($\alpha=1,2$), we expand them over the oscillator basis

$$\phi_{E-\mathcal{E}, l_\alpha}(y_\alpha) = \sum_{n_\alpha=0}^{N_0-1} C_{n_\alpha}^{(E-\mathcal{E}, l_\alpha)} \psi_{n_\alpha, l_\alpha}(y_\alpha, b), \quad (14)$$

where

$$\psi_{n_\alpha, l_\alpha}(y_\alpha, b) = (-1)^{n_\alpha} \mathcal{N}_{n_\alpha l_\alpha} \tilde{\rho}^{l_\alpha} e^{-\frac{1}{2}\tilde{\rho}^2} L_{n_\alpha}^{l_\alpha+1/2}(\tilde{\rho}^2), \quad (15)$$

$$\tilde{\rho} = \frac{y_\alpha}{b}, \quad \mathcal{N}_{n_\alpha l_\alpha} = \sqrt{\frac{2\Gamma(n_\alpha + 1)}{b^3 \Gamma(n_\alpha + l_\alpha + 3/2)}}$$

is an oscillator function and b is the oscillator length.

In eq. (14), a finite number of oscillator functions appears. But in fact, this expansion involves an infinite number of functions, since we know an asymptotic behavior of wave function $\phi_{E-\mathcal{E}, l_\alpha}(y_\alpha)$ in coordinate space and expansion coefficients $C_{n_\alpha}^{(E-\mathcal{E}, l_\alpha)}$ in oscillator space.

At large distances $x_1 \ll y_1$ between an α -particle and a ${}^5_\Lambda\text{He}$ subsystem being in the state with energy \mathcal{E}_1 wave function $\phi_{E-\mathcal{E}_1, l_1}(y_1)$ has the following form:

$$\phi_{E-\mathcal{E}_1, l_1}(y_1) \approx \delta_{c_0, c} \psi_{l_1}^{(-)}(k_1 y_1; \eta_1) - S_{c_0, c} \psi_{l_1}^{(+)}(k_1 y_1; \eta_1), \quad (16)$$

where $S_{c_0, c}$ is the scattering matrix, index c numerates an exit channel $c = \{\mathcal{E}_1 \lambda_1 l_1\}$ and c_0 indicates the entrance channel, $\psi_{l_1}^{(-)}$ ($\psi_{l_1}^{(+)}$) is the incoming (outgoing) Coulomb wave, and η_1 is Sommerfeld parameter. Determination of the incoming and outgoing Coulomb wave functions can be found, for instance, in Ref. [37].

The asymptotic behaviour of the wave function $\phi_{E-\mathcal{E}_2, l_2}(y_2)$ describing scattering of a Λ -hyperon on ${}^8\text{Be}$ subsystem being in the state with energy \mathcal{E}_2 is determined by a superposition of the Hankel functions $H_{l_2+1/2}^{(\pm)}$, since Λ -hyperon does not have an electric charge:

$$\phi_{E-\mathcal{E}_2, l_2}(y_2) \approx \delta_{c_0, c} H_{l_2+1/2}^{(-)}(k_2 y_2) - S_{c_0, c} H_{l_2+1/2}^{(+)}(k_2 y_2), \quad (17)$$

Parameters $k_{1,2}$ and η_1 in our case are defined as

$$k_{1,2} = \sqrt{\frac{2m(E - \mathcal{E}_{1,2})}{\hbar^2}},$$

$$\eta_1 = \frac{Z^2 e^2}{\sqrt{2(E - \mathcal{E}_{1,2})}} \sqrt{\frac{m}{\hbar^2} \frac{4(4 + \bar{m}_\Lambda)}{\bar{m}_\Lambda + 8}},$$

where $Z = 2$ is a charge of α -cluster, E is the total energy of three-cluster system ($E > \mathcal{E}_{1,2}$).

Having obtained all elements $S_{c, \bar{c}}$ of the scattering S matrix, we make the following steps to extract important physical information. First, we use one of the standard parametrizations of the S matrix:

$$S_{c, \bar{c}} = \eta_{c, \bar{c}} \exp\{2i\delta_{c, \bar{c}}\}.$$

The diagonal values of the phase shifts $\delta_{c, c}$ and inelastic parameters $\eta_{c, c}$ are analyzed to study elastic and inelastic processes in a many-channel system. Second, the S matrix $\|S_{c, \bar{c}}\|$ is reduced to the diagonal form or to the representation of the uncoupled channels. In this representation we obtain a set of eigenphase shifts δ_α which provides us with additional information on the processes under consideration. The eigenphase shifts δ_α also allow us to determine the total and partial widths of resonance states in the compound

system. The details of this scheme and its justifications can be found in Ref. [38].

For numerical investigations of the three-cluster system ${}^9_\lambda\text{Be}$, we have to use a finite basis of Gaussian and oscillator functions. As was pointed out above, N_G^{max} Gaussian functions give us the same number of eigenstates and corresponding eigenfunctions of a two-cluster Hamiltonian. To study effects of cluster polarization, we will involve different numbers of these eigenstates, their actual number we denote as N_G ($1 \leq N_G \leq N_G^{\text{max}}$).

Index N_f numerates a cumulative number of a basis function for the σ_α th eigenstate of the α th ($\alpha=1, 2$) two-cluster subsystem with energy $\mathcal{E}_{\sigma_\alpha}$ ($1 \leq \sigma_\alpha \leq N_G$) and for n_α oscillator quanta ($0 \leq n_\alpha \leq N_O - 1$):

$$\begin{aligned} N_f &= 1 + n_\alpha + (\sigma_\alpha - 1) N_O + (\alpha - 1) N_G N_O, \\ 1 &\leq N_f \leq 2N_G N_O. \end{aligned} \quad (18)$$

Thus, in our calculations we deal with the $2N_G$ -channel system for the case of two coupled binary configurations. In an isolated configuration approximation the number of channels equals N_G .

Traditionally, the spectrum of the bound states is obtained with the diagonalization of the three-cluster Hamiltonian with N_f basis functions. The diagonalization also reveals a large numbers of pseudo-bound states which are specific combinations of scattering states. In what follows, we are going to study both bound and pseudo-bound states.

To obtain scattering wave functions and elements of scattering S -matrix, we will solve a system of nonhomogeneous algebraic equations for the expansion coefficients. For scattering states, the number of oscillator functions N_O determines a border between an internal and asymptotic regions. It is obvious that the number of channels and the number of basis functions can be different for calculating bound and scattering states.

We usually perform two type of calculations of the bound and scattering states. In the first type of calculations we take into account polarizability of clusters involving maximal number of eigenstates of the two-cluster Hamiltonians, i.e. $1 \leq \sigma_\alpha \leq N_G^{\text{max}}$. This approach will be called the approach with “soft” clusters. The second type of calculations discards polarizability of clusters by involving only one eigenfunction ($\sigma_\alpha = 1$) of two-cluster Hamiltonians. It is obviously that in such a case clusters do not change their size and shape, and thus we call it the approach with “rigid” clusters.

3. Results and Discussions

In the present paper we restrict the discussion to the case of zero orbital momenta λ_α of binary subsystems ${}^5_\Lambda\text{He}$ and ${}^8\text{Be}$. Hence, orbital momentum l_α describing relative motion of the binary subsystems and the third cluster determines the total orbital momentum $L = l_\alpha$ and parity. Consequently, a state with a given total angular momentum and parity J^π corresponds to the only value of L . Namely, positive parity states are characterized by even values of L , while negative parity states correspond to the odd values of L . $J^\pi = 1/2^+$ states have zero total orbital momentum.

In many publications devoted to the hypernucleus ${}^9_\Lambda\text{Be}$, the bound and resonance states were marked by the total orbital momentum L and parity π , which was explained by a small contribution of the spin-orbit components of a Lambda-nucleon interaction. To make a bridge between this notation and ours, we will mark the states of ${}^9_\Lambda\text{Be}$ with three quantum numbers J , π and L in the following way $J^\pi(L)$.

In the asymptotic region we have taken into account two channels describing the scattering of an α -particle on ${}^5_\Lambda\text{He}$ subsystem and a Λ -hyperon on ${}^8\text{Be}$ subsystem, provided that both subsystems are in their ground states. In the internal region three more excited states for each subsystem have also been considered. Such an approximation allows for polarization of two-cluster subsystems due to the interaction with the third cluster at small distances between clusters, but at large distances binary subsystems can be only in their ground states.

3.1. Input parameters

First of all we need to select values for the input parameters. We perform and present two sets of calculations by using two different sets of input parameters. These sets realize two criteria for selecting input parameters which reproduce different observable quantities. We will denote two sets of input parameters $P1$ and $P2$, correspondingly. We start with the first set of the input parameters and in Subsections 3.2.1, 3.2.1 the main results will be discussed with the $P1$. In Subsection 3.2.3 we consider $P2$ set of input parameters.

We involve the modified Hasegawa-Nagata (MHNP) [39, 40] potential as a nucleon-nucleon interaction. We use the same nucleon-hyperon potential as in Ref. [41]. Parameters of the spin-orbit interaction of the ΛN interaction

are taken for the version NSC97f from Ref. [16]. In Fig. 1 we display the even components of the nucleon-hyperon potential.

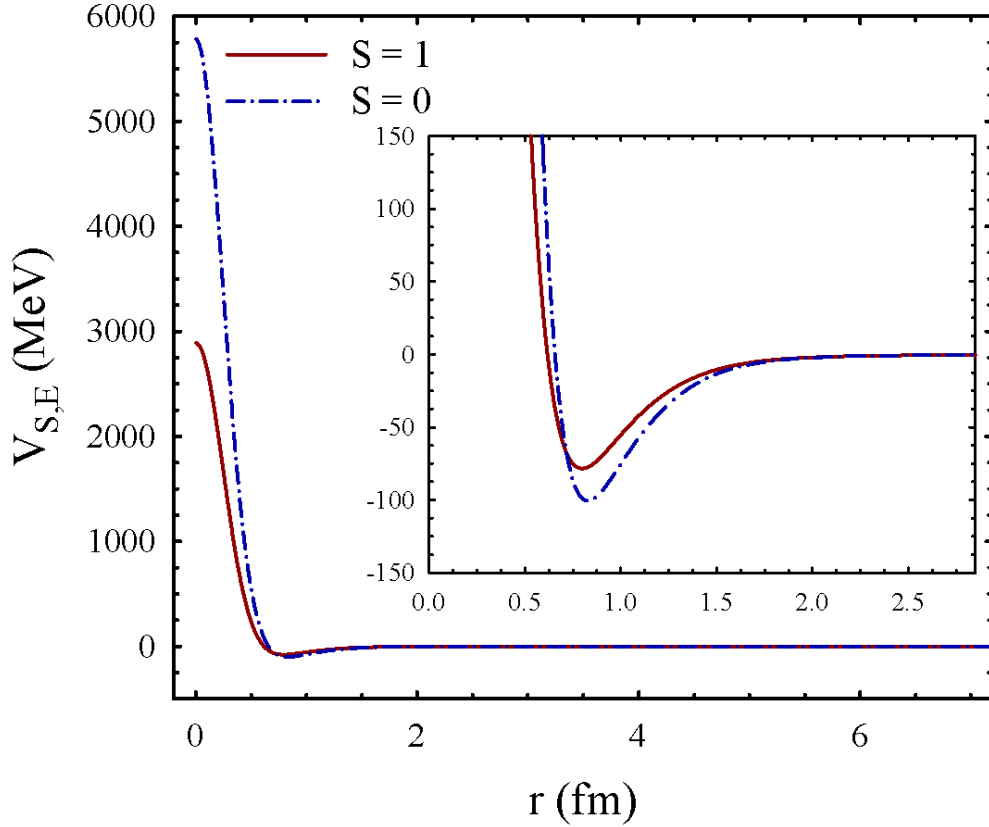


Figure 1: The even components of the central part of the $N\Lambda$ potential.

Traditionally we chose the oscillator length $b = 1.317$ fm to minimize the threshold energy of the two-cluster subsystems. The value $m = 0.4389$ of Majorana parameter of the MHNP is adjusted to reproduce the energy and width of the ground state in ${}^9\text{Be}$ nucleus relative to $\alpha + \alpha + n$ threshold. The standard value of the Majorana parameter is $m = 0.4057$. Cut-off parameter $k_{eff} = 0.889 \text{ fm}^{-1}$ of the ΛN -potential is selected to reproduce the energy of the ground state of ${}^9_{\Lambda}\text{Be}$ nucleus with respect to $\alpha + \alpha + \Lambda$ threshold.

Parameters b_{ν} ($\nu=1, 2, 3, 4$) of Gaussian functions are determined as

Table 1: Spectrum of resonance states in ${}^8\text{Be}$ calculated in a two-cluster model and compared with experimental data [42]

J^π	Theory		Experiment	
	E , MeV	Γ , MeV	E , MeV	Γ , MeV
0^+	0.859	0.958	0.092	5.57×10^{-6}
2^+	4.138	4.809	3.12	1.513
4^+	14.461	6.386	11.44	≈ 3.500

$b_\nu = b_0 q^{\nu-1}$. In $P1$ input parameter set, for ${}^5_\Lambda\text{He}$ we selected $b_0 = 0.7$ fm, $q = 1.85$, and for ${}^8\text{Be}$ we took $b_0 = 1.15$ fm, $q = 2.2$. Such values of the parameters minimize the ground state energies of the ${}^5_\Lambda\text{He}$ and ${}^8\text{Be}$ nuclei.

We have also invoked for the calculations another set of the input parameters ($P2$), which gives the experimental value -3.12 MeV for the binding energy of the ${}^5_\Lambda\text{He}$. Namely, we used different values of $b_0 = 0.25$ fm, $q = 1.85$ for the Gaussian functions describing the ${}^5_\Lambda\text{He}$ subsystem and slightly adjusted cut-off parameter $k_{eff} = 0.887$ fm $^{-1}$ of the ΛN -potential to reproduce the energy of the ground state of ${}^9_\Lambda\text{Be}$ nucleus with respect to $\alpha + \alpha + \Lambda$ threshold. Oscillator length $b = 1.317$ fm and the value $m = 0.4389$ of Majorana parameter of the MHNP and parameters of the Gaussian functions, describing the ${}^8\text{Be}$ subsystem, remained the same in $P2$ input parameter set.

Note, that with such values of oscillator length b and the Majorana parameter m of the MHNP we obtain resonance states of ${}^8\text{Be}$ which are presented in Table 1. In Table 1 we also show the experimental parameters of resonance states in ${}^8\text{Be}$. As we see, the theoretical results are in fairly good agreement with the available experimental data presented in Ref. [42]. It was indicated in Ref. [43] that these input parameters are not optimal for resonance structure of ${}^8\text{Be}$. The optimal values of b and m leads to overbinding the compound nucleus ${}^9\text{Be}$. This is a typical problem for many semi-realistic nucleon-nucleon potentials. Thus, in the present calculations we use those values of b and m which provide the correct position of the ${}^9\text{Be}$ ground state with respect to the three-cluster threshold $\alpha + \alpha + n$.

3.2. Spectrum of ${}^9_\Lambda\text{Be}$ nucleus

3.2.1. Convergence of parameters of resonance states, $P1$ input parameters

The spectrum of positive and negative parity states for $1/2 \leq J \leq 7/2$ ($0 \leq L \leq 4$) of the ${}^9_\Lambda\text{Be}$ nucleus calculated within the AMGOB model is presented in Tables 2, 3. Tables 2, 3 demonstrate that the polarization of

two-cluster subsystems plays an important role in formation of bound and resonance states of the ${}^9_{\Lambda}\text{Be}$. For the positive parity states, cluster polarization decreases energy of the bound and resonance states. It also reduces significantly total width of the resonance states. Cluster polarization, for example, decreases the energy of the ${}^9_{\Lambda}\text{Be}$ ground $1/2^+(0)$ state by 400 keV, and the energy of the $3/2_1^+(0)$ resonance state which determined in experiments as the second excited state is reduced by 245 keV, while its total width decreases more than 6 times. Similar situation with the $5/2_1^+(2)$ resonance state which has approximately the same energy. Cluster polarization shifts down the energy of the resonance state by 302 keV and causes an eightfold decrease in its width. Besides, allowing for polarization leads to the formation of a large number of narrow resonance states in three-cluster continuum above the decay threshold ${}^9_{\Lambda}\text{Be} \Rightarrow {}^8\text{Be}(0_2^+) + \Lambda$ located at 1.63 MeV above the three-cluster decay threshold.

For the negative parity states we observe from Table 3 that the parameters of the lowest $1/2_1^-(1)$ and $3/2_1^-(1)$ resonance states remain almost intact when cluster polarization is taken into account. The energy of this resonance is quite close to the energy 0.7 MeV where becomes possible ${}^8\text{Be}(0_1^+) + \Lambda$ scattering. Since the latter channel is considered properly already in the approximation of rigid two-cluster subsystems, allowing for cluster polarization does not change a lot the lowest $1/2_1^-(1)$ and $3/2_1^-(1)$ states. It might be well to point out that spectra of the $1/2^-(1)$ and $3/2^-(1)$ states are almost degenerate, because they are characterized by the same orbital momentum $L = 1$ and the spin-orbit interaction is small.

Analyzing partial widths of the resonance states tabulated in Tables 2 and 3 we can observe that the majority of the resonances decay via ${}^8\text{Be} + \Lambda$ channel. There are not more than 2 resonances decaying via ${}^5_{\Lambda}\text{He} + \alpha$ channel for a given value of J^π . In all the cases, except $5/2_6^-(3)$ and $7/2_6^-(3)$ resonances, partial widths via different channels significantly differ from one another. The above mentioned $5/2_6^-(3)$ and $7/2_6^-(3)$ states represent the only case when the resonances decay with almost equal probability via both channels. It is interesting to note also the principal change in partial widths of the lowest $1/2_1^+(0)$ resonance. Allowing for cluster polarization not only halves the energy of this resonance state, but also changes its dominant decay channel.

It was pointed out in Ref. [31] that the resonance states $1/2^-(1)$ and $3/2^-(1)$ in ${}^9_{\Lambda}\text{Be}$ form the "genuinely hypernuclear" rotational band as there is no such a band in the nucleus ${}^9\text{Be}$. The Pauli principle forbids the valence

Table 2: Spectrum of positive parity states of ${}^9_{\Lambda}\text{Be}$ nucleus obtained within the AMGOB model with $P1$ set of the input parameters taking into account cluster polarization (soft) or neglecting it (rigid). Γ is a total width of the resonance state, $\Gamma_{1,2}$ are partial decay widths of the resonance via ${}^5_{\Lambda}\text{He}+\alpha$ and ${}^8\text{Be}+\Lambda$ channels, correspondingly. Energy is given in MeV, the total and partial widths are in keV.

$J^{\pi}(L)$	rigid				soft			
	E	Γ	Γ_1	Γ_2	E	Γ	Γ_1	Γ_2
$1/2^+(0)$	-6.204				-6.623			
	5.360	3170	170	3000	1.792	3.3	2.3	1
					2.252	60.3	11.8	48.5
					2.733	384	0.6	383.4
					3.396	349.2	84.6	264.6
					4.107	213.6	23.3	190.3
					4.650	470.8	77.8	393
					5.083	10.8	8.4	2.4
$3/2^+(2)$	-3.297	35.8	35.8		-3.543	5.5	5.5	
					2.115	0.045	0.01	0.035
					2.850	0.027	0.01	0.017
					3.314	206.9	0.1	206.8
					3.886	8.3	2	6.3
					4.387	105.7	1.6	104.1
					5.212	26.2	4.3	21.9
					5.610	55.8	0.4	55.4
$5/2^+(2)$	-3.446	12	12		-3.748	0.75	0.75	
					2.115	0.043	0.01	0.033
					2.849	0.041	0.037	0.004
					3.312	210.42	0.07	210.35
					3.885	8.3	2	6.3
					4.386	107.8	1.3	106.5
					5.209	26.7	4.2	22.5
					5.630	57.64	0.17	57.4
$7/2^+(4)$	4.726	2962.5	2962.4	0.1	2.610	0.0091	0.0088	0.0003
					3.643	0.002	0.0007	0.0013
					3.979	8.302	0.001	8.301
					4.500	2625.2	2625.2	0.01
					5.139	1.6	0.09	1.51

Table 3: Spectrum of negative parity states of ${}^9_{\Lambda}\text{Be}$ nucleus obtained within the AMGOB model with $P1$ set of the input parameters taking into account cluster polarization (soft) or neglecting it (rigid). Γ is a total width of the resonance state, $\Gamma_{1,2}$ are partial decay widths of the resonance via ${}^5_{\Lambda}\text{He}+\alpha$ and ${}^8\text{Be}+\Lambda$ channels, correspondingly. Energy is given in MeV, the total and partial widths are in keV.

		rigid			soft			
$J^{\pi}(L)$	E	Γ	Γ_1	Γ_2	E	Γ	Γ_1	Γ_2
$1/2^-(1)$	0.723	4521	0.4	4520.6	0.724	4228.5	0.4	4228.1
					1.924	3.74	3.735	0.005
					2.519	30.1	21.1	9
					3.364	259.3	72.5	186.8
					4.350	250.8	0.1	250.7
					5.739	148.4	1.2	147.2
					5.906	91.3	2.9	88.4
$3/2^-(1)$	0.723	4507.4	0.4	4507	0.724	4213.7	0.5	4213.2
					1.924	3.99	3.97	0.02
					2.519	31.1	22	9.1
					3.368	258.6	72.3	186.3
					4.354	252.5	0.1	252.4
					5.733	154	10	144
					5.907	94.8	2.6	92.2
$5/2^-(3)$					2.345	0.132	0.003	0.129
					3.227	0.1157	0.0007	0.115
					4.117	54.1	0.6	53.5
					4.403	1.5	0.4	1.1
					5.133	42.5	11.4	31.1
					5.866	2.3	1.1	1.2
$7/2^-(3)$					2.345	0.145	0.001	0.144
					3.227	0.197	0.001	0.197
					4.117	54.3	0.6	53.7
					4.403	1.4	0.4	1
					5.132	41.7	11.5	30.2
					5.865	2.1	1.1	1

nucleon to occupy the lowest p orbitals in ${}^9\text{Be}$, while there is no such a restriction for the Λ particle in ${}^9_\Lambda\text{Be}$. In this respect it is interesting to note that there are two types of the positive and negative parity states as it follows from Tables 2 and 3. The first type comprises the resonance states with the dominant binary structure $\Lambda + {}^8\text{Be}$. Such resonance states have the partial width $\Gamma_2 > \Gamma_1$. They are created mainly by rotation of the Λ particle around ${}^8\text{Be}$. And they are "genuinely hypernuclear" states. In particular, we would like to note that our predictions concerning the energy and width of the lowest $1/2^-_1(1)$ and $3/2^-_1(1)$ resonance states strongly correlate with the results obtained in [31], since these states are located just near $\Lambda + {}^8\text{Be}$ and have quite large width.

The second type of states are represented by the resonance states with partial width $\Gamma_1 > \Gamma_2$. These resonance states decay mainly via $\alpha + {}^5_\Lambda\text{He}$ channel, where the Λ particle forms a bound state with an alpha particle. Rotation of the second alpha-particle around ${}^5_\Lambda\text{He}$ creates a set of resonance states of the positive and negative parity.

In the energy region considered $E \leq 6$ MeV above $2\alpha + \Lambda$ threshold four open channels could play a part in the formation of resonance states. They correspond to $\sigma = 1, 2$ eigenstates of the two-cluster subsystems calculated with four Gaussian functions and listed in Table 4. We can assume that appearance of narrow resonances in the case when cluster polarization is taken into account could result from coupling the channels belonging to the same cluster configuration: ${}^8\text{Be}(0^+_1) + \Lambda$ and ${}^8\text{Be}(0^+_2) + \Lambda$ channels, ${}^5_\Lambda\text{He}(0^+_1) + \alpha$ and ${}^5_\Lambda\text{He}(0^+_2) + \alpha$ channels. In particular, the first pair of the channels could be more coupled due to proximity of the energies needed to make the channels open.

Referring to Table 4 it will be observed that in our model ${}^5_\Lambda\text{He}$ subsystem is overbound by 0.9 MeV compared to its experimental binding energy. However, this overbinding is much smaller than in other simple model calculations based upon ΛN potentials [44].

In Table 4 we also display the mass root-mean-square radius for all bound and pseudo-bound states. As we see, the ground state of ${}^5_\Lambda\text{He}$ is a compact two-cluster system, while the lowest pseudo-bound state, representing the ground state of ${}^8\text{Be}$, is very dispersed with the large value of $r_m = 5.71$ fm. Dispersed are also states $\sigma = 2$ and $\sigma = 3$ of ${}^8\text{Be}$ and the state $\sigma = 2$ of ${}^5_\Lambda\text{He}$, however with the smaller values of r_m .

Table 4 shows also the average distances \bar{r}_α between clusters. They are

Table 4: Energy and mass root-mean-square radius of the two-cluster bound and pseudo-bound states with $P1$ set of the input parameters. The energy is measured from a two-cluster threshold indicated in the first column.

2C-system	Quantity	$\sigma = 1$	$\sigma = 2$	$\sigma = 3$	$\sigma = 4$
${}^5_{\Lambda}\text{He}=\alpha + \Lambda$	E , MeV	-4.06	2.91	21.12	139.76
	r_m , fm	1.71	3.25	2.20	1.48
	\bar{r}_α , fm	2.62	6.72	4.06	1.78
${}^8\text{Be}=\alpha + \alpha$	E , MeV	0.70	1.63	9.11	53.03
	r_m , fm	5.71	4.37	3.05	1.95
	\bar{r}_α , fm	15.16	7.07	2.34	1.39

determined in the following way

$$\bar{r}_\alpha = b\sqrt{\langle g_{\mathcal{E}_\sigma, \lambda_\alpha} | x_\alpha^2 | g_{\mathcal{E}_\sigma, \lambda_\alpha} \rangle / \mu_\alpha},$$

where μ_α is a reduced mass appearing in the definition of the Jacobi vector \mathbf{x}_α . The quantity \bar{r}_α gives the most probable relative distance between the interacting clusters. This quantity has been discussed in the literature. For example, in Ref. [11] devoted to the study of spectrum of p -shell hypernuclei including ${}^9_{\Lambda}\text{Be}$ within a microscopic cluster model, the average distance between two alpha particles in the ground state of ${}^8\text{Be}$ were determined approximately. It was obtained that $\bar{r}_\alpha=5.99$ fm which is smaller than our estimation $\bar{r}_\alpha=15.16$ fm. We believe that such a large difference for the average distance between alpha particles can be partially ascribed to different nucleon-nucleon potentials involved in Ref. [11] and in our calculations. But the main difference is related to the way how this quantity is determined. Note that detail investigation of the average distance between two alpha particles in different states of ${}^8\text{Be}$ has been performed in Ref. [45] within the two-cluster resonating group method.

3.2.2. Spectrum of the $3/2^+(2)$ states, $P1$ input parameters

In Fig. 2 we display the spectrum of the Hamiltonian for the $3/2^+(2)$ states obtained with $P1$ input parameter set. The spectrum is obtained in a single-configuration (SC) and coupled-configuration (CC) approximations. Eigenvalues of the Hamiltonian are shown as a function of the number of basis functions N_f defined by Eq. (18). It is necessary to recall that in the present calculations the single-configuration approximation involves four different channels with a binary subsystem in the ground and three excited

states. 200 oscillator functions are employed in each channel. Thus the region $1 \leq N_f \leq 800$ in both panels of Fig. 2 corresponds to the SC approximation, and the region $801 \leq N_f \leq 1600$ represents the CC approximation. The range $1 \leq N_f \leq 200$ shows the spectrum of eigenstates created by basis functions of the channel ${}^5_\Lambda\text{He}(0_1^+) + \alpha$ (left panel) and ${}^8\text{Be}(0_1^+) + \Lambda$ (right panel), the range $201 \leq N_f \leq 400$ display effects on the eigenspectrum of the second channel ${}^5_\Lambda\text{He}(0_2^+) + \alpha$ and ${}^8\text{Be}(0_2^+) + \Lambda$, correspondingly, and so on.

One can see that there are a large number of plateaus which appear in the SC and CC approximations. The dot-dashed lines indicate the position of the $3/2^+(2)$ resonance states, obtained by solving the dynamic equations with proper boundary conditions. Such a plateau can be a marker of a narrow

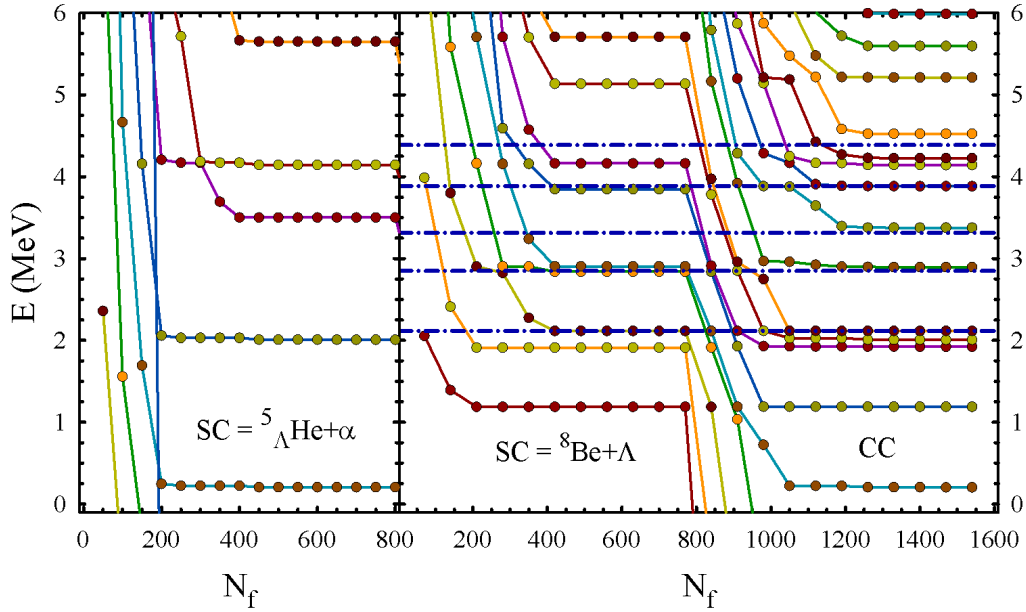


Figure 2: Spectrum of eigenstates of the internal part of Hamiltonian for $3/2^+(2)$ states constructed in a single-configuration (SC) and coupled-configuration (CC) approximations with $P1$ input parameters. The $3/2^+(2)$ resonance states are displayed by the dot-dashed line in the area of the CC approximation. Energy is measured from the three-cluster decay threshold $\alpha + \alpha + \Lambda$.

resonance state in the system under consideration. Besides, in many-channel systems the plateaus may appear due to a weak coupling of channels. It is

worthwhile noticing that the second type of plateau may appear, for example, when a weak spin-orbit interaction couples states with different values of the total orbital momentum L and/or total spin S (LS coupling scheme).

Many plateaus which are observed in Fig. 2 in the single-configuration approximations belong to the second type. Indeed, if we have a closer look at the spectrum we can see that the channel describing the interaction of the third cluster with the most compact two-cluster subsystem (${}^5_{\Lambda}\text{He}(0_1^+) + \alpha$ or ${}^8\text{Be}(0_1^+) + \Lambda$) is dominant and noticeably reduces the energy of the eigenstates. Second in importance to the eigenstates of the ${}^9_{\Lambda}\text{Be}$ hypernucleus are ${}^5_{\Lambda}\text{He}(0_2^+) + \alpha$ and ${}^8\text{Be}(0_2^+) + \Lambda$ channels. All other channels are weakly coupled to the dominant channels and thus contribute much less to the energy of the eigenstates shown in Fig. 2. The same is also valid for a number of plateaus occurring in the CC area. We can also see in Fig. 2 that in many cases the energy of resonance states is close to the energy of plateau. The narrower is a resonance state, the closer is its energy to the plateau energy.

Table 5: Spectrum of $J^\pi(L) = 3/2^+(2)$ states of ${}^9_{\Lambda}\text{Be}$ nucleus obtained within the AMGOB model with $P1$ set of the input parameters for different degree of polarization of two-cluster subsystems. Energy is in MeV and width is in keV.

$N_G = 1$		$N_G = 2$		$N_G = 3$		$N_G = 4$	
E	Γ	E	Γ	E	Γ	E	Γ
-3.297	35.8	-3.430	13.9	-3.539	5.6	-3.543	5.5
		2.115	0.08	2.115	0.08	2.115	0.04
		2.850	0.125	2.850	0.02	2.850	0.03
		3.319	197.6	3.314	206.9	3.3136	206.9
		3.887	9.4	3.886	8.3	3.886	8.3
		4.387	104.5	4.387	105.7	4.387	105.7
		5.217	32.1	5.212	26.2	5.212	26.2
		5.643	68.6	5.630	55.8	5.630	55.8

As Table 5 suggests, the qualitative change of the spectrum is caused by taking into account the 0_2^+ state in ${}^5_{\Lambda}\text{He}$ and ${}^8\text{Be}$ subsystem. Allowing for higher excited states leads only to some slight alteration of energies and widths, but does not change the number of resonances. From this fact, we might reason that 0_2^+ states of the binary subsystems plays a large part in the structure of resonance states of ${}^9_{\Lambda}\text{Be}$ nucleus.

In Table 6 we compare spectrum of the $3/2^+(2)$ resonance states obtained with and without Coulomb forces. 200 oscillator functions are used in both

calculations. The results presented in Table 6 allow us to reveal effects of the

Table 6: Effects of the Coulomb forces on the energy and width of the $3/2^+(2)$ resonance states studied with $P1$ set of the input parameters.

with Coulomb		without Coulomb	
E , MeV	Γ , keV	E , MeV	Γ , keV
-3.543	5.5	-5.103	0
2.115	0.04	1.129	1.122
2.850	0.03	1.865	0.107
3.314	206.9	2.764	29.034
3.886	8.3	3.126	64.264

Coulomb forces on energy and width of the resonance states in ${}^9_\Lambda\text{Be}$, and to understand peculiarities of the present model.

We can conclude from Table 6 that without the Coulomb forces energy of all the resonance states is decreased by approximately 1 MeV, and the lowest $3/2^+(2)$ resonance state with $E = -3.542$ MeV below the three-cluster threshold is transformed into a bound state. It is interesting to note that the Coulomb interaction makes $3/2^+(2)$ resonance state wider and other resonance states narrower.

Figure 3 illustrates the behaviour of the phase shifts of elastic scattering for $J^\pi(L) = 3/2^+(2)$ states of ${}^9_\Lambda\text{Be}$ hypernucleus for two sets of the input parameters. We can observe from Fig. 3 a large impact of cluster polarization on the phase shifts of elastic scattering. It is interesting to note that the phase shift of ${}^5_\Lambda\text{He}(0^+) + {}^4\text{He}$ scattering calculated with $P1$ input parameters manifests resonance behaviour only for the lowest $3/2^+(2)$ state and the $3/2^+(2)$. All other resonances in $P1$ calculations become apparent only in the behaviour of ${}^8\text{Be}(0^+) + \Lambda$ scattering phase.

3.2.3. Spectrum of ${}^9_\Lambda\text{Be}$ for $P2$ set of the input parameters

The spectrum of positive and negative parity states for $1/2 \leq J \leq 7/2$ ($0 \leq L \leq 4$) of the ${}^9_\Lambda\text{Be}$ nucleus calculated within the AMGOB model for $P2$ set of the input parameters is presented in Tables 7, 8. Only 41 keV above the ${}^5_\Lambda\text{He} + \alpha$ decay threshold appears a narrow $1/2^+(0)$ resonance with the width of 9 keV. This state was absent in $P1$ calculations.

In Fig. 4 we compare spectra of bound and resonance states of the hypernucleus ${}^9_\Lambda\text{Be}$ which lie below the $\alpha + \alpha + \Lambda$ threshold and are obtained with $P1$ and $P2$ sets of input parameters. These spectra are calculated with cluster

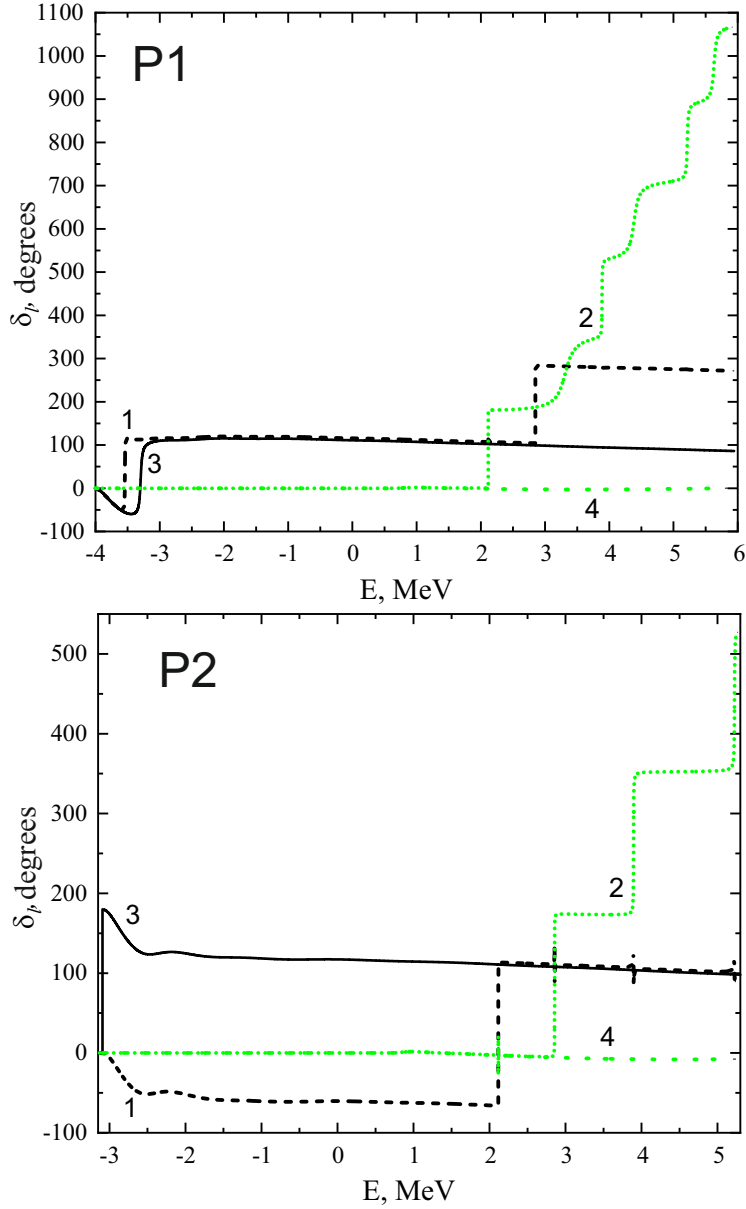


Figure 3: Phase shifts of elastic many-channel scattering for $J^\pi(L) = 3/2^+(2)$ states of ${}^9_\Lambda\text{Be}$ versus energy in the ${}^5_\Lambda\text{He}(0_1^+) + {}^4\text{He}$ (1, 3) and ${}^8\text{Be}(0_1^+) + \Lambda$ (2, 4) channels. The data are obtained with $P1$ (upper panel) and $P2$ (lower panel) set of input parameters for soft (1, 2) and rigid (3, 4) two-cluster subsystems. Orbital momenta of the relative motion of clusters l_1 and l_2 equals 2.

polarization. One sees that the $P2$ set of input parameters shifts noticeable the energy of the ${}^5_{\Lambda}\text{He}+\alpha$ threshold and slightly shifts up energies of $3/2^+$ (2) and $5/2^+$ (2) states. And thus these states are transformed into the bound states lying close to the ${}^5_{\Lambda}\text{He}+\alpha$ threshold. Neglecting cluster polarization turns bound $3/2^+$ (2) state into a virtual state, while $5/2^+$ (2) remains to be bound with respect to the ${}^5_{\Lambda}\text{He}+\alpha$ threshold.

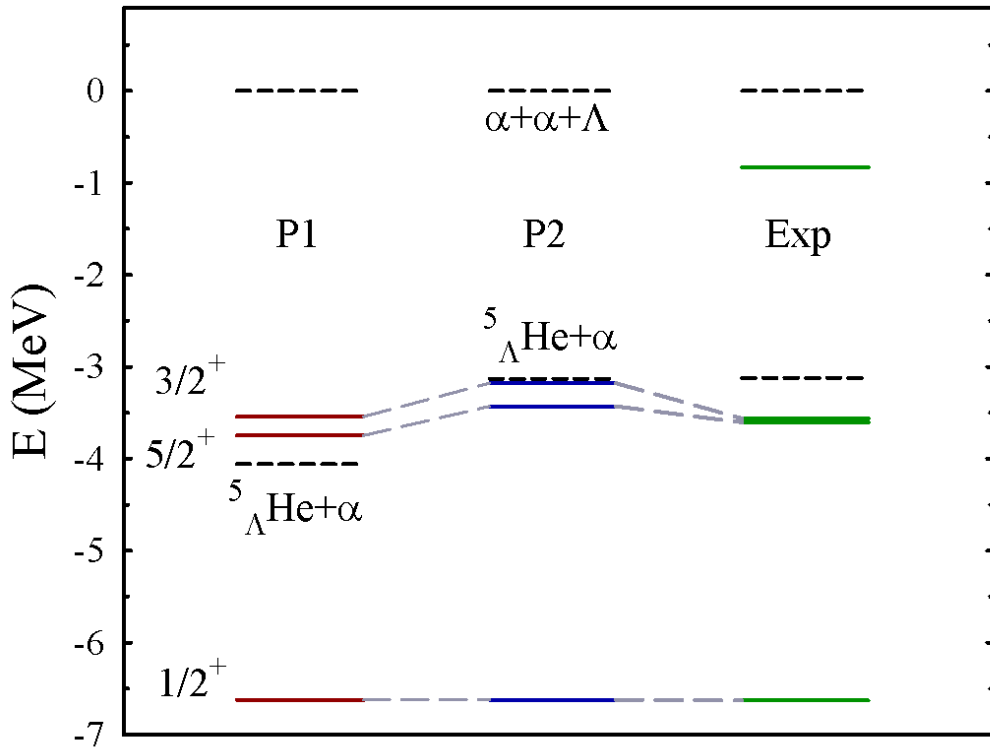


Figure 4: Energy of bound and resonance states in ${}^9_{\Lambda}\text{Be}$ obtained with two sets of input parameters $P1$ and $P2$ and compared to the experimental data (Exp) from Refs. [51, 19]

Comparing the data presented in Tables 7, 8 with those listed in Tables 2, 3 we observe that $P2$ set of input parameters generates half as many resonances as $P1$ set. Besides, the majority of the resonances presented in Tables 7, 8 decay mainly via ${}^5_{\Lambda}\text{He}+\alpha$ channel, while $P1$ set of parameters produced the resonances decaying into ${}^8\text{Be}+\Lambda$ channel. Furthermore, almost all res-

onances (except $7/2^+(4)$ case), which disappeared in $P2$ calculations, have larger widths and are characterized with partial width $\Gamma_2 \gg \Gamma_1$. The $7/2^+(4)$ wide resonance appeared to be almost insensitive both to the different sets of input parameters and to the accounting of cluster polarization. All narrow $7/2^+(4)$ resonances did not appear in $P2$ calculations.

Table 7: Spectrum of positive parity states of ${}^9_\Lambda\text{Be}$ nucleus obtained within the AMGOB model with $P2$ input parameter set taking into account cluster polarization (soft) or neglecting it (rigid). Γ is a total width of the resonance state, $\Gamma_{1,2}$ are partial decay widths of the resonance via ${}^5_\Lambda\text{He}+\alpha$ and ${}^8\text{Be}+\Lambda$ channels, correspondingly. Energy is given in MeV, the total and partial widths are in keV.

$J^\pi(L)$	rigid				soft			
	E	Γ	Γ_1	Γ_2	E	Γ	Γ_1	Γ_2
$1/2^+(0)$	-6.33				-6.62			
	-3.01	95	95		-3.089	9	9	
					1.82	13.9	6.7	7.2
					2.391	49.2	21.2	28
					3.309	91.2	47.5	43.7
					4.482	84.7	74.7	10
$3/2^+(2)$					4.5	85.5	83	2.5
	-3.09	0.001	0.001		-3.179			
					2.116	0.36	0.22	0.14
					2.856	2.84	10.2	18.2
					3.895	10.3	3.9	6.4
$5/2^+(2)$					5.22	18.2	8	10.2
	-3.34				-3.43			
					2.116	0.35	0.21	0.14
					2.856	2.70	0.93	1.77
$7/2^+(4)$					3.894	9.87	3.67	6.2
					5.22	17.7	7.6	10.1
	4.67	2295.1	2295.09	0.02	4.658	2283	2282.98	0.02

Energies of the ${}^5_\Lambda\text{He}$ bound and pseudo-bound states obtained for $P2$ set of input parameters tabulated in Table 9. We can observe from Table 9 that the energy of the bound state corresponds to its experimental value, while all the pseudo-bound states have much higher energies than in $P1$ calculations. Probably, this means that polarization of the ${}^5_\Lambda\text{He}$ subsystem hardly affects the spectrum of the ${}^9_\Lambda\text{Be}$ hypernucleus, resulting in a smaller

Table 8: Spectrum of negative parity states of ${}^9_{\Lambda}\text{Be}$ nucleus obtained within the AMGOB model with $P2$ input parameter set taking into account cluster polarization (soft) or neglecting it (rigid). Γ is a total width of the resonance state, $\Gamma_{1,2}$ are partial decay widths of the resonance via ${}^5_{\Lambda}\text{He}+\alpha$ and ${}^8\text{Be}+\Lambda$ channels, correspondingly. Energy is given in MeV, the total and partial widths are in keV.

$J^{\pi}(L)$	rigid				soft			
	E	Γ	Γ_1	Γ_2	E	Γ	Γ_1	Γ_2
$1/2^-(1)$				1.934	7.37	6.32	1.05	
				2.574	36.29	31.29	5	
				3.554	75.1	68.8	6.3	
				4.837	85.47	84.84	0.63	
$3/2^-(1)$				1.934	7.46	6.83	0.63	
				2.574	35.78	31.44	4.34	
				3.554	73.68	68.44	5.24	
				4.837	85.59	85.31	0.28	
$5/2^-(3)$				2.345	0.06	0.059	0.001	
				3.228	0.13	0.07	0.06	
				4.40	0.74	0.36	0.38	
$7/2^-(3)$				2.345	0.083	0.082	0.001	
				3.228	0.126	0.072	0.054	
				4.40	0.72	0.37	0.35	

Table 9: Energy and mass root-mean-square radius of the ${}^5_{\Lambda}\text{He}=\alpha + \Lambda$ bound and pseudo-bound states obtained for $P2$ set of input parameters. The energy is measured from the two-cluster threshold indicated in the first column.

2C-system	Quantity	$\sigma = 1$	$\sigma = 2$	$\sigma = 3$	$\sigma = 4$
${}^5_{\Lambda}\text{He}=\alpha + \Lambda$	E , MeV	-3.13	57.99	300.07	1013.10
	r_m , fm	1.53	1.52	1.33	1.28

number of resonances in the ${}^9_{\Lambda}\text{Be}$ for the $P2$ calculations.

3.2.4. Comparison with other methods and experiment

In Table 10 we display the spectrum of ${}^9_{\Lambda}\text{Be}$ obtained in Refs. [46] and [47], and compare it with our results.

Table 10: Spectrum of bound and resonance states in ${}^9_{\Lambda}\text{Be}$ obtained in different models. Energy is displayed in MeV, width is given in keV.

	[46]			Present paper, P1			Present paper, P2			[47]		
L^{π}	E	Γ	J^{π}	E	Γ	J^{π}	E	Γ	J^{π}	E	Γ	
0^+	-6.65	-	$\frac{1}{2}^+$	-6.62	-	$\frac{1}{2}^+$	-6.62	-	$\frac{1}{2}^+$	-7.13	-	
2^+	-3.82	-	$\frac{5}{2}^+$	-3.75	0.75	$\frac{5}{2}^+$	-3.43	-	$\frac{5}{2}^+$	-3.89	-	
			$\frac{3}{2}^+$	-3.54	5.5	$\frac{3}{2}^+$	-3.18	-	$\frac{3}{2}^+$	-3.89	-	
1^-	0.1	2500	$\frac{1}{2}^-$	0.724	4228	$\frac{1}{2}^+$	-3.09	9	$\frac{3}{2}^-$	-2.94	120	
			$\frac{3}{2}^-$	1.92	4.0	$\frac{3}{2}^-$	1.93	7.46	$\frac{3}{2}^-$	-2.21	2160	
			$\frac{3}{2}^-$	3.37	258.6	$\frac{3}{2}^-$	3.55	73.68	$\frac{3}{2}^-$	3.86	5.6	
4^+	3.2	780	$\frac{7}{2}^+$	2.61	0.01	$\frac{7}{2}^+$	4.66	2283				
3^-	8.0	6100	$\frac{7}{2}^-$	2.35	0.15	$\frac{7}{2}^-$	2.35	0.08				

As this nucleus has not more than two bound states and a large number of resonance states, we selected those investigations which determined both energies and widths of the excited states.

In Ref. [46] a three-cluster model with an approximate treatment of the Pauli principle was employed. The $\alpha\Lambda$ interaction was determined in a folding approximation with the same ΛN potential as in the present paper, however another value of the parameter k_F ($k_F = 0.963 \text{ fm}^{-1}$) was selected. The complex scaling method was involved in Ref. [46] to locate the energy and width of resonance states.

As the spin-orbit interaction is disregarded in Ref. [46], the authors labelled the states of the ${}^9_{\Lambda}\text{Be}$ with the total orbital momentum L . The energy of the ground state, obtained in Ref. [46] is close to our results. There is also a certain likeness of our results for both input parameter sets and the results of Ref. [46] for the energy of the 2_1^+ state. However, in our approach this state is split by spin-orbit interaction on two states - $5/2_1^+(2)$ and $3/2_1^+(2)$. In $P1$ calculations these states are resonances, since they are located above the lowest ${}^5_{\Lambda}\text{He}(0_1^+) + \Lambda$ threshold, while with $P2$ input parameters these states are bound. An important point is that our model reproduce the correct order of the $5/2_1^+(2)$ and $3/2_1^+(2)$ states and only slightly overestimates their splitting for both sets of the input parameters.

The $L^\pi = 1^-$ resonance state presented in Ref. [46] corresponds to the lowest $1/2_1^-(1)$ resonance obtained in our model with $P1$ set of the input parameters. Both states are located close to the $2\alpha + \Lambda$ and have a large width.

There are some differences in the position and in the widths of other resonance states. The energy of the 4^+ resonance listed in Ref.[46] is about 0.6 MeV higher the energy of the lowest $7/2^+(4)$ resonance obtained with $P1$ input parameter set of our model and a significantly larger width. At the same time, $7/2^+(4)$ resonance produced by $P2$ input parameter set is characterized by higher energy and larger width than the 4^+ resonance from Ref. [46]. Finally, the lowest $7/2^-(3)$ resonance state produced by both sets of input parameters in our model have essentially lower energy and smaller width than the 3^- resonance presented in Ref. [46].

The Faddeev equation methodology were applied in Ref. [47] to study bound and resonance states in ${}^9_{\Lambda}\text{Be}$ within a macroscopic three-body model. Several effective $\alpha\Lambda$ interactions and a separable $\alpha\alpha$ interaction were involved to calculate the spectrum. The selected $\alpha\Lambda$ and $\alpha\alpha$ interactions lead to the overbound ground state of ${}^9_{\Lambda}\text{Be}$ in Ref. [47]. As the spin-orbit interaction is neglected in [47], the $3/2^+$ and $5/2^+$ have the same energy. They are bound states, since they are located under the ${}^5_{\Lambda}\text{He}+\alpha$ threshold. Three $3/2^-$ resonance states were found in Ref. [47], two of them are located bellow the three-cluster threshold and one above. $P2$ set of the input parameters of our model produces the lowest $1/2_1^+(1)$ resonance with the energy close to the energy of the lowest $3/2^-$ resonance from Ref. [47]. The $3/2_3^-$ state from [47] lies near our $3/2^-$ resonance states with energy 3.37 MeV and 3.55 MeV for $P1$ and $P2$ input parameter set, correspondingly. The latter states have, however, larger widths than the width of the $3/2_3^-$ resonance state obtained

in Ref. [47].

In Table 11 we collected experimental data on the spectrum of the ${}^9_{\Lambda}\text{Be}$ hypernucleus. The references are found in Ref. [46]. As we can see from Table

Table 11: Spectrum of ${}^9_{\Lambda}\text{Be}$ identified in different experiments compared with our results. Energy is given in MeV

Source	[48, 49]	[20, 50]	[51, 19]	Theory, P1	Theory, P2
J^{π}	E	E	J^{π}	J^{π}	J^{π}
$1/2^+$	-6.63	-5.90	$1/2^+$	$1/2_1^+$	$1/2_1^+$
			$5/2_1^+$	$5/2_1^+$	$5/2^+$
$3/2^+$	-3.55	-2.97	$3/2^+$	$3/2_1^+$	$3/2_1^+$
		-0.10		$1/2_1^-$	$1/2_2^+$
				$5/2_3^+$	$5/2_3^+$
				$3/2_3^+$	$3/2_3^+$
				$3/2_4^-$	$3/2_3^-$
		3.62			

11, there is some consistency in experimental data only for the energies of the ground $1/2^+$ state and excited $3/2^+$, $5/2^+$ states. The energies of these three levels obtained within our model are in a good agreement with the experimental data from the first and last column. Energy of the lowest $3/2_1^-$ state obtained with $P1$ input parameter set is closer to the experimental value than that produced in $P2$ calculations. However, in the latter case $3/2_1^-$ and $5/2_1^-$ are located below the ${}^5_{\Lambda}\text{He}+\alpha$ decay threshold, in accordance with the experimental data, while in $P1$ calculations these states lie above the two-cluster threshold. Energies of the $3/2_3^+$ and $5/2_3^+$ resonance states are close to the experimentally observed level with $E = 2.89$ MeV from Ref. [51, 19]. Finally, the resonance state with energy $E = 3.62$ MeV reported in [20, 50] is located near our $3/2_4^-$ and $3/2_3^-$ resonances generated by $P1$ and $P2$ input parameter sets, correspondingly.

3.3. Nature of the resonance states

As we can see above, our model generates a large number of resonance states in ${}^9_{\Lambda}\text{Be}$. What is the nature of such resonance states? What factors are responsible for the appearance of these resonance states? All the results of this Subsection have been obtained with $P1$ set of the input parameters, since this variant of calculations produces more resonance states.

There are at least three possible reasons for the formation of resonance states and thus three types of resonances emerged in our many-channel model

of ${}^9_{\Lambda}\text{Be}$. First, the so-called shape resonance states can be created by a centrifugal or the Coulomb barriers, or by a combination of both barriers.

The centrifugal barrier is present in both ${}^5_{\Lambda}\text{He}+\alpha$ and ${}^8\text{Be}+\Lambda$ channels, if the total orbital momentum and parity allow rotational states with nonzero orbital momentum of relative motion of the interacting clusters. The Coulomb barrier is present in the ${}^5_{\Lambda}\text{He}+\alpha$ channel only. Effects of the Coulomb forces on parameters of the resonance states are demonstrated in Table 6 with $J^{\pi} = 3/2^{+}$ states. This example shows us that the Coulomb interaction is not responsible for creating such a rich variety of resonance states. As we have seen, it changes parameters of a resonance state and transforms a weakly bound state into a resonance state.

Second, some part of the obtained resonance states may be considered as the Pauli resonance states. Appearance of a large number of resonance states in cluster systems has been discovered many years ago (see, for example, Refs. [52, 53, 54, 55, 56, 57, 58, 59]). In Refs. [60, 61] it has been shown with a simple two-cluster model systems how the Pauli resonances appear in the resonating group method calculations when different oscillator lengths are used for the interacting clusters. It is worthwhile noticing that with distinct values of oscillator lengths for different clusters one achieves more adequate description of a compound system. The Pauli resonance states may appear also in the case when the same oscillator lengths are used but more advanced internal cluster functions are adopted. Using different oscillator lengths implies invoking monopole excitations of each cluster. Such excitations in light nuclei have the energy around 20 MeV. And, consequently, the Pauli resonances appear in a high-energy range. Meanwhile, employment of more advanced wave functions of interacting clusters by considering them as a binary structure may result in a set of low-energy internal states which generate the Pauli resonances at a low energy. That is the case for the present investigation.

The Pauli resonances is caused by the almost Pauli forbidden states, which can be present in the wave function instead of the Pauli forbidden states both in the case of different oscillator lengths and advanced intrinsic cluster wave function. Recall that the forbidden states are the eigenfunctions of the norm kernel with zero eigenvalues, while the almost Pauli forbidden states correspond to nonzero but very small eigenvalues. In Ref. [62] it was claimed that the Pauli resonances disappear if the almost forbidden states are removed from the wave function. It was demonstrated for the ${}^{16}\text{O}+\alpha$ scattering that by omitting the eigenstates with eigenvalues less than

1.0×10^{-2} one removes the Pauli resonances. We apply this algorithm to calculate the $3/2^+(2)$ phase shifts and parameters of the resonance states. In this case we have got only one almost forbidden state with the eigenvalue 6.4×10^{-8} . Other eigenvalues are spread in the region between 0.2 and 1.8. Elimination of the almost forbidden state did not result in changing phase shifts and parameters of the $3/2^+(2)$ resonances. The same results were obtained for the $1/2^+(0)$ and $1/2^-(1)$ states. This let us conclude that the obtained resonances are not the Pauli resonances. We suggest that the Pauli resonance states arise at a higher energy.

Third, Feshbach resonances appear in many-channel systems, provided that the channels have different threshold energies (see original papers of Feshbach [63, 64], a review in Ref. [65] and Ref. [66], where the Feshbach resonance state was discovered in ^{11}Li considered as a three-body system $^9\text{Li}+n+n$). The Feshbach resonance originates from a bound states in one of the channels with a higher energy of the decay threshold. Having coupled with other channel(s) with lower threshold energy, the bound state may then decay through the open channel(s). If the coupling between channels is weak, the bound state turns into a resonance state. If the coupling is strong, a bound state can be dissolved by continuum. We have the necessary conditions for creation of the Feshbach resonance states, since the binary channels involved in the calculations have different threshold energies (see Table 4). In the region $1 \text{ MeV} < E < 6 \text{ MeV}$, where we discovered the majority of the resonance states, there are four closed channels which can generate bound states.

However, to prove that our resonance states are the Feshbach resonances, we need to compare spectrum of the resonance states with the spectrum of bound states in closed binary channels treated separately. To obtain spectrum of the bound states, we selected from a huge matrix of the Hamiltonian those blocks which describe each channel and omitted the blocks which couple them. Thus problem of the N_{ch} coupled channels are reduced to the problem of N_{ch} independent channels and each channel is treated separately. As we pointed above, there is a weak coupling between different channels of ^9Be . Thus we expect a correspondence between energies of the bound and resonance states.

Comparison is made in Fig. 5 where we display the energy of the $3/2^+(2)$ resonance states created by the eight coupled channels (the middle spectrum) with the energy of bound states in the channel $^5\text{He}(0_3^+)+\alpha$ (the left spectrum) and channel $^8\text{Be}(0_3^+)+\Lambda$ (the right spectrum). We display only those

bound states in all closed channels which lie in the energy range of our interest. Spectrum of bound states in each channel is obtained with 200 oscillator functions. By the dashed lines we indicated two- and three-body thresholds.

One can see in Fig. 5 that the energies of the resonance states obtained in the coupled-channel approximation are very close to the energies of the bound states calculated within a single-channel approximation. It is necessary to recall that the threshold energies of the channels ${}^5_{\Lambda}\text{He}(0_3^+) + \alpha$ and ${}^8\text{Be}(0_3^+) + \Lambda$ equal 21.12 and 9.11 MeV, correspondingly, as it was indicated in Table 4. And thus all energy levels, which are obtained in the single-channel approximations and lay below these threshold energies, are bound states. The ${}^5_{\Lambda}\text{He}(0_3^+) + \alpha$ closed channel generates three resonance states, while the ${}^8\text{Be}(0_3^+) + \Lambda$ closed channel creates four resonance states. Thus, the numerous resonance states emerged from our calculations are mainly the Feshbach resonance states. They complement the shape resonance states created by the centrifugal and Coulomb barriers which appear at the low-energy region. From Fig. 5 one may conclude that the coupling of open channels with the ${}^5_{\Lambda}\text{He}(0_3^+) + \alpha$ is stronger than with the ${}^8\text{Be}(0_3^+) + \Lambda$, since the resonance states are shifted noticeably with respect to the corresponding bound states in the first channel but not with respect to the states of the second channel.

Summarizing, we can conclude that the location of narrow resonances of the ${}^9_{\Lambda}\text{Be}$ hypernucleus in the energy region above ${}^8\text{Be}(0_1^+) + \Lambda$ threshold depends on the pseudo-bound states of the ${}^8\text{Be}$ and ${}^5_{\Lambda}\text{He}$ two-cluster subsystems, which have been taken into account. We can assume that the experimentally observed levels of the two-body subsystems of the considered hypernucleus should be primarily accounted for. For the ${}^9_{\Lambda}\text{Be}$ hypernucleus these are 0^+ ground state and 2^+ , 4^+ resonance states of the ${}^8\text{Be}$ nucleus, as well as the 0^+ ground state of the ${}^5_{\Lambda}\text{He}$ hypernucleus. In the present paper, we properly accounted for the ground states of both two-body subsystems in the ${}^9_{\Lambda}\text{Be}$ hypernucleus. In addition, we allowed for both subsystems to be polarized without changing their angular momenta. There are strong grounds to believe that the location of the resonances of the ${}^9_{\Lambda}\text{Be}$ located below ${}^8\text{Be}(0_1^+) + \Lambda$ threshold remains unaffected by considering 2^+ and 4^+ pseudo-bound states of the ${}^8\text{Be}$ subsystem instead of already taken into account 0_2^+ , 0_3^+ and 0_4^+ states. However, it can change the energies of the ${}^9_{\Lambda}\text{Be}$ resonance states lying at the energy range $E > 2$ MeV above the three-cluster threshold.

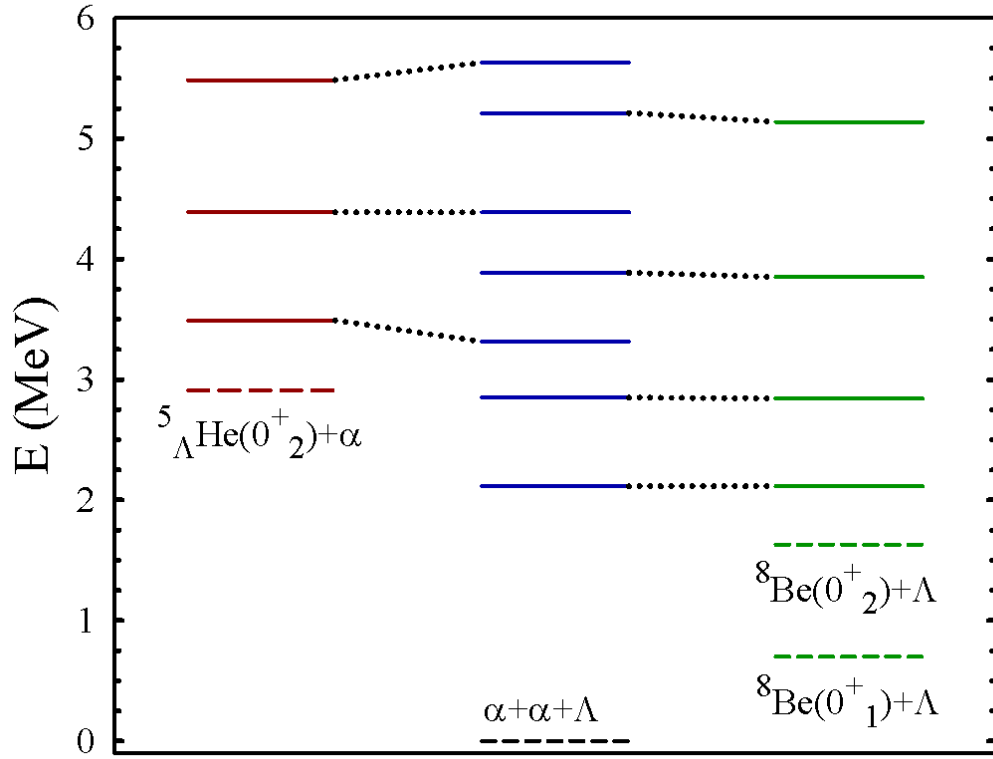


Figure 5: Spectrum of the $3/2^+(2)$ resonance states in ${}^9_{\Lambda}\text{Be}$ obtained in the coupled-channel approximation compared with the bound states created by closed binary channels ${}^5_{\Lambda}\text{He}(0^+_3)+\alpha$ (the left spectrum) and ${}^8\text{Be}(0^+_3)+\Lambda$ (the right spectrum) treated separately. $P1$ set of the input parameters was used.

4. Conclusions

We have applied a microscopic three-cluster model to studying the structure of the ${}^9_{\Lambda}\text{Be}$ hypernucleus. The model treats correctly the Pauli principle and accounts for polarization of two-cluster subsystems of the hypernucleus when the third cluster is close by reducing a three-cluster problem to a coupled many-channel two-cluster problem. A Gaussian basis was used for the description of the two-cluster subsystems, while a harmonic oscillator basis was invoked for the relative motion of the two-cluster subsystem and the remaining cluster.

The hypernucleus ${}^9_{\Lambda}\text{Be}$ was considered as a three-cluster system comprising of two alpha particles and a Λ -hyperon. Within the present model the three-cluster configuration was projected on two binary configurations ${}^5_{\Lambda}\text{He}+\alpha$ and ${}^8\text{Be}+\Lambda$, provided that ${}^5_{\Lambda}\text{He}$ and ${}^8\text{Be}$ were described as two-cluster systems. A finite number of Gaussian functions were used to describe $\alpha - \Lambda$ and $\alpha - \alpha$ binary subsystems. This resulted in a discretization of the continuous spectrum of ${}^5_{\Lambda}\text{He}$ and ${}^8\text{Be}$. The set of pseudo-bound states in ${}^5_{\Lambda}\text{He}$ and ${}^8\text{Be}$ allowed us to take into account polarizability of these systems.

The spectrum of bound and resonance states in the ${}^9_{\Lambda}\text{Be}$ hypernucleus was studied in detail. Calculations have been performed with two set of input parameters. Both sets were selected to reproduce the ground state energy of ${}^9_{\Lambda}\text{Be}$ and to minimize the energy of the ${}^8\text{Be}$ two-cluster subsystem of this hypernucleus. At the same time, *P2* input parameter set was determined to reproduce the binding energy of ${}^5_{\Lambda}\text{He}$ with respect to its $\alpha + \Lambda$ decay threshold, while *P1* input parameter set minimizes binding energy of ${}^5_{\Lambda}\text{He}$ making it slightly overbound.

It was shown that the cluster polarizability plays a significant role in formation of bound and resonance states of this hypernucleus. Moreover, polarization of the two-cluster subsystems on interaction with the third cluster is responsible for creation of a large number of resonance states, a large part of them are very narrow with the total width less than 100 keV. We have shown that the majority of the narrow resonances in the energy range $1 \text{ MeV} < E < 6 \text{ MeV}$ are the Feshbach resonances generated due to a weak coupling of different binary channels in ${}^9_{\Lambda}\text{Be}$. *P2* set of the input parameters generate the less number of resonance states than *P1* set due to higher energies of pseudo-bound states in ${}^5_{\Lambda}\text{He}$.

There is a fairly good agreement between our results and available experimental data. However, in our calculations with the first set of input

parameters $P1$, the first $3/2^+(2)$ excited state of the ${}^9_{\Lambda}\text{Be}$ is a resonance state, since it is located above the lowest ${}^5_{\Lambda}\text{He}+\alpha$ decay threshold of the ${}^9_{\Lambda}\text{Be}$. This can be ascribed to the selected nucleon-nucleon and nucleon-hyperon potentials which slightly overbind the ${}^5_{\Lambda}\text{He}$ subsystem. At the same time, $P2$ set of the input parameters make the first $3/2^+(2)$ and $5/2^+(2)$ states to be bound in accordance with the experiment. The order of lowest $5/2^+(2)$ and $3/2^+(2)$ levels corresponds to the experimental data for both sets of the input parameters. There is a very good correspondence of the predicted by our model energies of the $3/2_3^+$ and $5/2_3^+$ resonance states to the experimentally observed level with $E = 2.89$ MeV from Ref. [51, 19].

5. Acknowledgment

This work was supported in part by the Program of Fundamental Research of the Physics and Astronomy Department of the National Academy of Sciences of Ukraine (Project No. 0117U000239).

References

- [1] V. S. Vasilevsky, F. Arickx, J. Broeckhove, T. P. Kovalenko, A microscopic three-cluster model with nuclear polarization applied to the resonances of ${}^7\text{Be}$ and the reaction ${}^6\text{Li}(p, {}^3\text{He}){}^4\text{He}$, Nucl. Phys. A 824 (1-4) (2009) 37–57. arXiv:0807.0136, doi:10.1016/j.nuclphysa.2009.03.011.
- [2] A. V. Nesterov, V. S. Vasilevsky, T. P. Kovalenko, Effect of cluster polarization on the spectrum of the ${}^7\text{Li}$ nucleus and on the reaction ${}^6\text{Li}(n, {}^3\text{H}){}^4\text{He}$, Phys. Atom. Nucl. 72 (2009) 1450–1464. doi:10.1134/S1063778809090051.
- [3] A. V. Nesterov, V. S. Vasilevsky, T. P. Kovalenko, Spectrum of bound states of nucleus ${}^{10}\text{B}$ in a three-cluster microscopic model, Ukr. J. Phys. 59 (11) (2014) 1065–1077.
- [4] Y. A. Lashko, G. F. Filippov, V. S. Vasilevsky, Microscopic three-cluster model of ${}^{10}\text{Be}$, Nucl. Phys. A 958 (2017) 78–100. doi:10.1016/j.nuclphysa.2016.11.004.

- [5] V. S. Vasilevsky, N. Takibayev, A. D. Duisenbay, Microscopic description of ${}^8\text{Li}$ and ${}^8\text{B}$ nuclei within three-cluster model, *Ukr. J. Phys.* 62 (6) (2017) 461–472.
- [6] V. S. Vasilevsky, A. V. Nesterov, T. P. Kovalenko, Three-cluster model of radiative capture reactions in seven-nucleon systems. Effects of cluster polarization., *Phys. Atom. Nucl.* 75 (7) (2012) 818–831.
- [7] E. Hiyama, T. Yamada, Structure of light hypernuclei, *Prog. Part. Nucl. Phys.* 63 (2) (2009) 339–395. doi:10.1016/j.ppnp.2009.05.001.
- [8] E. Hiyama, Y. Kino, M. Kamimura, Gaussian expansion method for few-body systems, *Prog. Part. Nucl. Phys.* 51 (1) (2003) 223–307. doi:10.1016/S0146-6410(03)90015-9.
- [9] E. Hiyama, M. Kamimura, Study of various few-body systems using Gaussian expansion method (GEM), *Frontiers of Physics* 13 (6) (2018) 132106. arXiv:1809.02619, doi:10.1007/s11467-018-0828-5.
- [10] Y. Kanada-En'yo, Structures of p -shell double- Λ hypernuclei studied with microscopic cluster models, *Phys. Rev. C* 97 (3) (2018) 034324. arXiv:1801.01259, doi:10.1103/PhysRevC.97.034324.
- [11] Y. Kanada-En'yo, Excitation energy shift and size difference of low-energy levels in p -shell Λ hypernuclei, *Phys. Rev. C* 97 (2) (2018) 024330. arXiv:1709.03375, doi:10.1103/PhysRevC.97.024330.
- [12] R. Wirth, D. Gazda, P. Navrátil, R. Roth, Hypernuclear no-core shell model, *Phys. Rev. C* 97 (6) (2018) 064315. arXiv:1712.05694, doi:10.1103/PhysRevC.97.064315.
- [13] L. L. Margolin, Microscopic investigation of the structure characteristics and wave functions of the five-body hypernucleus He_λ^5 , in: *European Physical Journal Web of Conferences*, Vol. 66, 2014, p. Di. doi:10.1051/epjconf/20146609013.
- [14] E. Hiyama, Y. Yamamoto, T. Motoba, M. Kamimura, Structure of $A=7$ iso-triplet Λ hypernuclei studied with the four-body cluster model, *Phys. Rev. C* 80 (5) (2009) 054321. arXiv:0911.4013, doi:10.1103/PhysRevC.80.054321.

- [15] O. Portilho, ${}^9_{\Lambda\Lambda}\text{Be}$ hypernucleus in the four-body model, *J. Phys. G Nucl. Phys.* 25 (5) (1999) 961–969. doi:10.1088/0954-3899/25/5/001.
- [16] E. Hiyama, M. Kamimura, T. Motoba, T. Yamada, Y. Yamamoto, ΛN Spin-Orbit Splittings in ${}^9_{\Lambda}\text{Be}$ and ${}^{13}_{\Lambda}\text{C}$ Studied with One-Boson-Exchange ΛN Interactions, *Phys. Rev. Lett.* 85 (2) (2000) 270–273. doi:10.1103/PhysRevLett.85.270.
- [17] T. Yamada, K. Ikeda, H. Band, T. Motoba, Cluster model theory of the ${}^9_{\Lambda}\text{Be}$ hypernucleus, *Phys. Rev. C* 38 (2) (1988) 854–866. doi:10.1103/PhysRevC.38.854.
- [18] Y. Funaki, T. Yamada, E. Hiyama, B. Zhou, K. Ikeda, Container structure of alpha-alpha-Lambda clusters in 9-Lambda-Beryrium, *Prog. Theor. Exp. Phys.* 2014 (11) (2014) 113D01. arXiv:1405.6067, doi:10.1093/ptep/ptu143.
- [19] H. Akikawa, S. Ajimura, R. E. Chrien, P. M. Eugenio, G. B. Franklin, J. Franz, L. Gang, K. Imai, P. Khaustov, M. May, Hypernuclear Fine Structure in ${}^9_{\Lambda}\text{Be}$, *Phys. Rev. Lett.* 88 (8) (2002) 082501. doi:10.1103/PhysRevLett.88.082501.
- [20] O. Hashimoto, H. Tamura, Spectroscopy of Λ hypernuclei, *Prog. Part. Nucl. Phys.* 57 (2) (2006) 564–653. doi:10.1016/j.ppnp.2005.07.001.
- [21] M. Isaka, M. Kimura, Impurity effects of the Λ particle on the 2 α cluster states of ${}^9\text{Be}$ and ${}^{10}\text{Be}$, *Phys. Rev. C* 92 (4) (2015) 044326. arXiv:1506.07238, doi:10.1103/PhysRevC.92.044326.
- [22] W.-Y. Li, J.-W. Cui, X.-R. Zhou, Structure of ${}^9_{\Lambda}\text{Be}$ and ${}^{10}_{\Lambda\Lambda}\text{Be}$ using the beyond-mean-field Skyrme-Hartree-Fock approach, *Phys. Rev. C* 97 (3) (2018) 034302. doi:10.1103/PhysRevC.97.034302.
- [23] M. Isaka, M. Kimura, A. Dote, A. Ohnishi, Deformation of hypernuclei studied with antisymmetrized molecular dynamics, *Phys. Rev. C* 83 (4) (2011) 044323. arXiv:1104.3940, doi:10.1103/PhysRevC.83.044323.
- [24] A. Feliciello, T. Nagae, Experimental review of hypernuclear physics: recent achievements and future perspectives, *Rep. Prog. Phys.* 78 (9) (2015) 096301. doi:10.1088/0034-4885/78/9/096301.

- [25] P. Veselý, E. Hiyama, J. Hrtánková, J. Mareš, Sensitivity of Λ single-particle energies to the ΛN spin-orbit coupling and to nuclear core structure in p-shell and sd-shell hypernuclei, *Nucl. Phys. A* 954 (2016) 260–272. [arXiv:1605.05646](#), [doi:10.1016/j.nuclphysa.2016.05.013](#).
- [26] M. Theeten, D. Baye, P. Descouvemont, Three-body models of the ${}^6_{\Lambda\Lambda}\text{He}$ and ${}^9_{\Lambda}\text{Be}$ hypernuclei with non-local interactions, *Nucl. Phys. A* 753 (1) (2005) 233–248. [doi:10.1016/j.nuclphysa.2005.02.129](#).
- [27] Y. Fujiwara, K. Miyagawa, M. Kohno, Y. Suzuki, D. Baye, J. M. Sparenberg, Faddeev calculation of 3α and $\alpha\alpha\Lambda$ systems using $\alpha\alpha$ resonating-group method kernels, *Phys. Rev. C* 70 (2) (2004) 024002. [arXiv:nucl-th/0404071](#), [doi:10.1103/PhysRevC.70.024002](#).
- [28] Y. Fujiwara, M. Kohno, K. Miyagawa, Y. Suzuki, Spin-orbit splitting of ${}^9_{\Lambda}\text{Be}$ excited states studied with the SU_6 quark-model baryon-baryon interactions, *Phys. Rev. C* 70 (4) (2004) 047002. [arXiv:nucl-th/0407039](#), [doi:10.1103/PhysRevC.70.047002](#).
- [29] E. Hiyama, M. Kamimura, T. Motoba, T. Yamada, Y. Yamamoto, Three- and Four-Body Cluster Models of Hypernuclei Using the G-Matrix ΛN Interaction – ${}^9_{\Lambda}\text{Be}$, ${}^{13}_{\Lambda}\text{C}$, ${}^6_{\Lambda\Lambda}\text{He}$ and ${}^{10}_{\Lambda\Lambda}\text{Be}$ –, *Prog. Theor. Phys.* 97 (6) (1997) 881–899. [doi:10.1143/PTP.97.881](#).
- [30] J. Lee, Q. Wu, Y. Funaki, H. Zong, E. Hiyama, Three-Body Structure of ${}^9_{\Lambda}\text{Be}$ with $\alpha + \alpha + \Lambda$ Cluster Model, *Few-Body Systems* 60 (2) (2019) 30. [doi:10.1007/s00601-019-1502-3](#).
- [31] T. Motoba, H. Bandō, K. Ikeda, T. Yamada, Chapter III. \Production, Structure and Decay of Light p-Shell Lambda-Hypernuclei, *Prog. Theor. Phys. Suppl.* 81 (1985) 42–103. [doi:10.1143/PTPS.81.42](#).
- [32] H. Bando, K. Ikeda, T. Motoba, Coupling Features in ${}^9_{\Lambda}\text{Be}$, ${}^{13}_{\Lambda}\text{C}$ and ${}^{21}_{\Lambda}\text{Ne}$ Hypernuclei, *Prog. Theor. Phys.* 69 (3) (1983) 918–928. [doi:10.1143/PTP.69.918](#).
- [33] K. Ikeda, H. Bandō, T. Motoba, Chapter V. \Multi-Strange Hypernuclei, *Prog. Theor. Phys. Suppl.* 81 (1985) 147–180. [doi:10.1143/PTPS.81.147](#).

- [34] I. N. Filikhin, S. L. Yakovlev, $\Lambda\Lambda^6\text{He}$ and $\Lambda^9\text{Be}$ Systems in the Three-Body Cluster Model Treated on the Basis of Differential Faddeev Equations, *Physics of Atomic Nuclei* 63 (3) (2000) 336–342. doi:10.1134/1.855640.
- [35] R. Wirth, D. Gazda, P. Navrátil, A. Calci, J. Langhammer, R. Roth, Ab Initio Description of p -Shell Hypernuclei, *Phys. Rev. Lett.* 113 (19) (2014) 192502. arXiv:1403.3067, doi:10.1103/PhysRevLett.113.192502.
- [36] J. Haidenbauer, U.-G. Meißner, Jülich hyperon-nucleon model revisited, *Phys. Rev. C* 72 (4) (2005) 044005. arXiv:nucl-th/0506019, doi:10.1103/PhysRevC.72.044005.
- [37] R. F. Barrett, B. A. Robson, W. Tobocman, Calculable methods for many-body scattering, *Rev. Mod. Phys.* 55 (1983) 155–243. doi:10.1103/RevModPhys.55.155.
- [38] J. Broeckhove, F. Arickx, P. Hellinckx, V. S. Vasilevsky, A. V. Nesterov, The ^5H resonance structure studied with a three-cluster J -matrix model, *J. Phys. G Nucl. Phys.* 34 (9) (2007) 1955–1970. doi:10.1088/0954-3899/34/9/008.
- [39] A. Hasegawa, S. Nagata, Ground state of ^6Li , *Prog. Theor. Phys.* 45 (1971) 1786–1807. doi:10.1143/PTP.45.1786.
- [40] F. Tanabe, A. Tohsaki, R. Tamagaki, $\alpha\alpha$ scattering at intermediate energies, *Prog. Theor. Phys.* 53 (1975) 677–691. doi:10.1143/PTP.53.677.
- [41] E. Hiyama, Y. Yamamoto, T. A. Rijken, T. Motoba, Four-body structure of $^7_\Lambda\text{Li}$ and ΛN spin-dependent interaction, *Phys. Rev. C* 74 (5) (2006) 054312. arXiv:nucl-th/0610019, doi:10.1103/PhysRevC.74.054312.
- [42] D. R. Tilley, J. H. Kelley, J. L. Godwin, D. J. Millener, J. E. Purcell, C. G. Sheu, H. R. Weller, Energy levels of light nuclei $A=8, 9, 10$, *Nucl. Phys. A* 745 (2004) 155–362. doi:10.1016/j.nuclphysa.2004.09.059.
- [43] V. S. Vasilevsky, K. Katō, N. Takibayev, Formation and decay of resonance states in ^9Be and ^9B nuclei: Microscopic three-cluster model

- investigations, *Phys. Rev. C* 96 (3) (2017) 034322. [arXiv:1706.05514](#), [doi:10.1103/PhysRevC.96.034322](#).
- [44] B. F. Gibson, I. Hungerford, E. V., A survey of hypernuclear physics, *Phys. Rep.* 257 (6) (1995) 349–388. [doi:10.1016/0370-1573\(94\)00114-I](#).
- [45] V. O. Kurmangaliyeva, N. Kalzhigitov, N. Takibayev, V. S. Vasilevsky, Resonance structure of ${}^8\text{Be}$ with the two-cluster resonating group method, *arXiv e-prints* (2020) [arXiv:2006.04525](#)[arXiv:2006.04525](#).
- [46] J. Lee, Q. Wu, Y. Funaki, H. Zong, E. Hiyama, Three-Body Structure of $\hat{9}_{\Lambda}\text{Be}$ with $\alpha\alpha\Lambda$ Cluster Model, *Few-Body Syst.* 60 (2) (2019) 30. [doi:10.1007/s00601-019-1502-3](#).
- [47] S. Oryu, H. Kamada, H. Sekine, H. Yamashita, M. Nakazawa, Calculation of ${}^9_{\Lambda}\text{Be}$ in an $\alpha\text{-}\alpha\text{-}\Lambda$ Three-Body Model Using the Faddeev Equations, *Few-Body Syst.* 28 (2) (2000) 103–129. [doi:10.1007/s006010070026](#).
- [48] M. May, S. Bart, S. Chen, R. E. Chrien, D. Maurizio, P. Pile, Y. Xu, R. Hackenburg, E. Hungerford, H. Piekarz, Y. Xue, M. Deutsch, J. Piekarz, P. D. Barnes, G. Franklin, R. Grace, C. Maher, R. Rieder, J. Szymanski, W. Wharton, R. L. Stearns, B. Bassalleck, B. Budick, Observation of Hypernuclear Gamma-Ray Transitions in ${}^7_{\Lambda}\text{Li}$ and ${}^9_{\Lambda}\text{Be}$, *Phys. Rev. Lett.* 51 (23) (1983) 2085–2088. [doi:10.1103/PhysRevLett.51.2085](#).
- [49] W. Brückner, B. Granz, D. Ingham, K. Kilian, U. Lynen, J. Niewisch, B. Pietrzyk, B. Povh, H. G. Ritter, H. Schröder, Strangeness exchange reaction on nuclei, *Phy. Lett. B* 62 (4) (1976) 481–484. [doi:10.1016/0370-2693\(76\)90689-4](#).
- [50] S. Ajimura, K. Aoki, H. Bhang, T. Endo, Y. Fujii, O. Hashimoto, H. Hotchi, E. Hungerford, J. H. Kim, Y. D. Kim, T. Kishimoto, K. Koshino, K. Kubota, K. Maeda, T. Nagae, H. Noumi, Y. Ohta, K. Omata, H. Outa, H. Park, Y. Saito, T. Saito, Y. Sato, M. Sekimoto, T. Shibata, T. Takahashi, T. Tamagawa, H. Tamura, L. Tang, H. Tanida, M. Youn, The (π^+, K^+) reaction and light Λ hypernuclear

- spectroscopy, Nucl. Phys. A 639 (1-2) (1998) 93–102. doi:10.1016/S0375-9474(98)00255-3.
- [51] H. Tamura, S. Ajimura, H. Akikawa, D. E. Alburger, K. Aoki, A. Banu, R. E. Chrien, G. B. Franklin, J. Franz, Y. Fujii, γ -ray spectroscopy in Λ hypernuclei, Nucl. Phys. A 754 (2005) 58–69. arXiv:nucl-ex/0411028, doi:10.1016/j.nuclphysa.2005.01.034.
- [52] D. R. Thompson, Y. C. Tang, Study of α +d and α +d* Systems with the Resonating-Group Method, Phys. Rev. 179 (4) (1969) 971–981. doi:10.1103/PhysRev.179.971.
- [53] D. R. Thompson, Y. C. Tang, Distortion Effects in d+ α System, Phys. Rev. C 8 (5) (1973) 1649–1664. doi:10.1103/PhysRevC.8.1649.
- [54] D. Clement, E. W. Schmid, A. G. Teufel, Positive energy bound states in resonating group calculations, Phys. Lett. B 49 (4) (1974) 308–310. doi:10.1016/0370-2693(74)90166-X.
- [55] D. J. Stubeda, Y. Fujiwara, Y. C. Tang, N+⁶Li system with flexible cluster wave function, Phys. Rev. C 26 (6) (1982) 2410–2416. doi:10.1103/PhysRevC.26.2410.
- [56] H. Kanada, T. Kaneko, Y. C. Tang, Specific distortion effects in ³H + α and ³He + α systems, Nucl. Phys. A 380 (1) (1982) 87–110. doi:10.1016/0375-9474(82)90584-X.
- [57] H. Walliser, T. Fliessbach, The oscillator frequency in resonating-group-method calculations, Nucl. Phys. A 394 (3) (1983) 387–396. doi:10.1016/0375-9474(83)90112-4.
- [58] H. Walliser, T. Fliessbach, Y. C. Tang, Resonating-group-method calculation for the α -¹⁶O system with realistic oscillator frequencies, Nucl. Phys. A 437 (2) (1985) 367–380. doi:10.1016/S0375-9474(85)90095-8.
- [59] H. Kanada, T. Kaneko, Y. C. Tang, Convergence features in the pseudostate theory of the d+ α system, Phys. Rev. C 38 (5) (1988) 2013–2018. doi:10.1103/PhysRevC.38.2013.

- [60] T. Fliessbach, H. Walliser, The structure of the resonating group equation, Nucl. Phys. A 377 (1) (1982) 84–104. doi:10.1016/0375-9474(82)90322-0.
- [61] H. Kanada, T. Kaneko, S. Saito, Effect Due to the Pauli Principle and Channel Coupling —Inner Repulsive Effect and Resonance-Like Contribution—, Prog. Theor. Phys. 54 (3) (1975) 747–757. doi:10.1143/PTP.54.747.
- [62] M. Kruglanski, D. Baye, Elimination of Pauli resonances in the generator-coordinate description of scattering, Nucl. Phys. A 548 (1) (1992) 39–48. doi:10.1016/0375-9474(92)90075-U.
- [63] H. Feshbach, Unified theory of nuclear reactions, Ann. Phys. 5 (4) (1958) 357–390. doi:10.1016/0003-4916(58)90007-1.
- [64] H. Feshbach, A unified theory of nuclear reactions. II, Ann. Phys. 19 (2) (1962) 287–313. doi:10.1016/0003-4916(62)90221-X.
- [65] C. Chin, R. Grimm, P. Julienne, E. Tiesinga, Feshbach resonances in ultracold gases, Rev. Mod. Phys. 82 (2) (2010) 1225–1286. doi:10.1103/RevModPhys.82.1225.
- [66] T. Matsumoto, J. Tanaka, K. Ogata, Borromean Feshbach resonance in ^{11}Li studied via $^{11}\text{Li}(p,p')$, Prog. Theor. Exp. Phys. 2019 (12) (2019) 123D02. doi:10.1093/ptep/ptz126.